AIAA JOURNAL
Vol. 46, No. 1, January 2008

Some Aeroelastic and Nonlinear Vibration Problems Encountered on the Journey to Ithaca

John Dugundji*
Massachusetts Institute of Technology, Cambridge, Massachusetts 02139

DOI: 10.2514/1.31958

The present paper describes three basic aeroelastic and nonlinear vibration problems investigated by the author and his students: namely, 1) stall flutter and nonlinear divergence of a two-dimensional flat-plate wing, 2) nonlinear vibrations of a clamped and a buckled beam, and 3) dynamic stability of a pendulum under parametric excitation. All of these problems seemed simple and were easily modeled experimentally and analytically. Yet they revealed some fundamental and interesting characteristics of nonlinear aeroelastic and vibration behavior of structures. Some experimental data are presented here that still remain to be resolved.

Nomenclature

A	=	beam section area
A_F	=	$w_{Bo}\omega_o/h\omega_1$ straight, w_{Bo}/ha buckled
a	=	w_c/h, $(2\omega_1/\omega_F)^2$
$\bar{a}$	=	parameter
a_1, b_1, a_2	=	response coefficients
$\dot{a}_1$, $\dot{b}_1$	=	$da_1/d\tau$, etc.
C_M	=	static moment coefficient
c	=	chord
E	=	modulus of elasticity
g	=	acceleration of gravity
h	=	beam thickness
I	=	mass moment of inertia, beam moment of inertia
K	=	1.818
k	=	response frequency index
k_α	=	torsional spring constant
L	=	length of the pendulum, length of the beam
m	=	mass/unit length, k/n
N_o	=	initial tension force
N_x	=	beam tension force
n	=	forcing frequency index
$P_{\rm cr}$	=	$4\pi^2 EI/L^2$
q	=	$3w_0/L$
q_1, q, $\tilde{q}$	=	generalized coordinates
r_i	=	$\sqrt{x_i^2 + y_i^2}$
S	=	flat-plate area
t	=	time
V	=	velocity
w	=	beam displacement
w_{Bo}	=	base displacement amplitude
w_c	=	initial center displacement, $w_o(L/2)$
w_o	=	initial buckled beam displacement, pendulum forcing amplitude
x	=	length coordinate
x_k, y_k	=	amplitude coefficients
α	=	angle of attack, $(\omega_1/\omega_F)^2$
α_o	=	initial angle
α_s	=	static equilibrium angle
ζ	=	critical damping ratio
ζ_T	=	total critical damping ratio
θ	=	pendulum angle
θ_o	=	initial pendulum angle
ρ	=	air density
τ	=	dimensionless time, $\omega_F t/n$, $\omega_F t/2$
ϕ	=	initial conditions for θ_o
ϕ_B	=	beam buckling mode
ϕ_1	=	beam first vibration mode
Ω	=	ω_F/ω_1
ω	=	torsional frequency
ω_F	=	forcing frequency
ω_o	=	natural frequency with no midplane force
ω_1	=	natural frequency with midplane force, pendulum natural frequency, $\sqrt{3g/2L}$

Presented as a paper at the 48th AIAA/ASME/ASCE/AHS/ASC Structures, Structural Dynamics, and Materials Conference, Honolulu, HI, 23–26 April 2007; received 10 May 2007; revision received 10 September 2007; accepted for publication 12 September 2007.

*Professor Emeritus, Department of Aeronautics and Astronautics. Associate Fellow AIAA.

I. Introduction

I WOULD like to start this paper with the opening lines from a poem named "Ithaca," by the modern Greek poet, Constantine P. Cavafy [1]. This poem comments on the long ten-year voyage of the ancient Greek hero, Odysseus (also known as Ulysses), to finally reach his home in Ithaca after the Trojan War. It begins like this,

> When you start on your journey to Ithaca,
> then pray that the road is long, full of adventure, full of knowledge.
> Do not fear the Lestrygonians and the Cyclopes and the angry Poseidon.
> You will never meet such as these on your path,
> if your thoughts remain lofty, if a fine
> emotion touches your body and your spirit.
> You will never meet the Lestrygonians, the Cyclopes and the fierce Poseidon,
> if you do not carry them within your soul,
> if your soul does not raise them up before you.
> Then pray that the road is long.
> That the summer mornings are many,
> that you will enter ports seen for the first time
> With such pleasure, with such joy!

Now I would like to present some interesting aeroelastic and nonlinear vibration problems that were encountered along my journey to Ithaca. Some of the aeroelastic problems are mentioned in a brief survey paper written a few years ago [2]. But here, I would like to focus on three interesting related problems encountered with my students along the way: namely, 1) stall flutter and nonlinear divergence of a 2-D flat-plate wing, 2) nonlinear vibrations of a clamped beam and a buckled beam, and 3) dynamic stability of a pendulum under parametric excitation.

All of these problems seemed simple and were easily modeled experimentally and analytically. Yet they revealed some fundamental and interesting characteristics of nonlinear aeroelastic

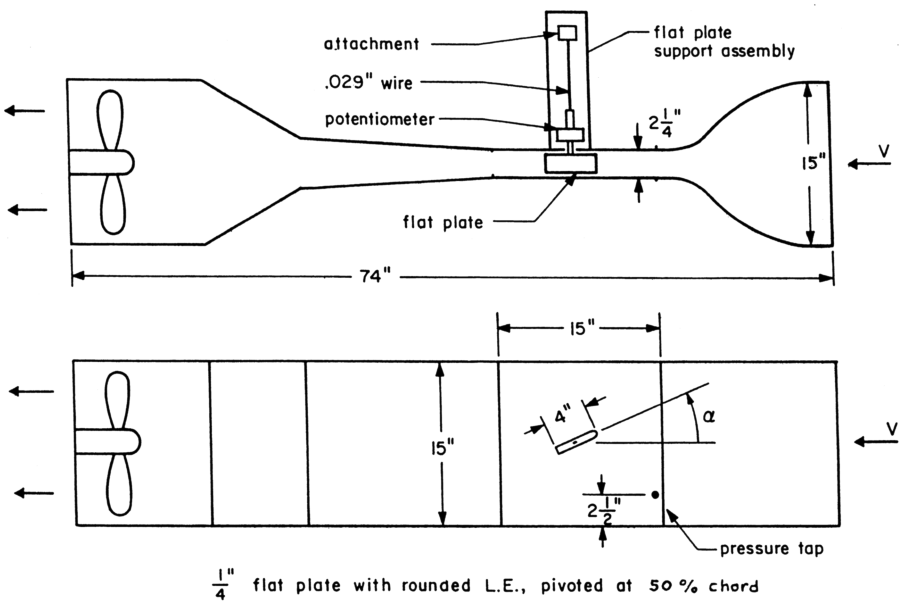

Fig. 1 General layout of the flutter experiment.

and vibration behavior of structures. Some details of their behavior still remain to be resolved.

II. Stall Flutter and Nonlinear Divergence of a Flat Plate

An experimental investigation was made of the nonlinear static divergence and stall flutter of a two-dimensional flat plate, pivoted about the midchord. The small flat plate had a chord of 4 in., a span of $2\frac{1}{4}$ in., and was placed between the upper and lower walls of a small wind tunnel, 15 in. apart, as shown in Fig. 1. The flat plate was $\frac{1}{4}$ in. thick, had a rounded leading edge, and was restrained in pitch about the midchord by a thin steel wire in torsion, which allowed a linear spring behavior over about ± 100 deg. The measured spring rate was 0.0115 ft · lb/rad. Thus, the only nonlinearity present was aerodynamic. Also, the initial angle of attack α_o could be set to any angle between 0 and 90 deg by rotating the flat-plate support assembly. One side wall of the small wind tunnel was made of Plexiglas for easy viewing of the flat plate, whereas the other side had a removable 15 × 15 in. wood panel to which the test model and its support assembly was attached. The flutter test model and support assembly was originally conceived and built by Frank Durgin of the Aeronautics and Astronautics department of the Massachusetts Institute of Technology and was later improved and extensively tested by the author and subsequent students.

The static behavior of the plate was investigated by first measuring the static moment coefficient C_M versus angle of attack α over a wide range of angles. This was accomplished by replacing the thin wire restraint by a relatively thick wire and using a strain gage measuring device. Figure 2 gives the resulting C_M versus α results, which show a sharp stalling characteristic around 10 deg.[†] The static equilibrium position of the flat plate is governed by the equation

$$\tfrac{1}{2}\rho V^2 S c C_M = k_\alpha(\alpha - \alpha_o) \tag{1}$$

The final nonlinear static equilibrium angle α_s of the flat plate is then readily found from these C_M versus α results by a simple graphical solution, as shown in Fig. 3. The resulting analytic and the observed experimental results for the nonlinear static divergence characteristics of the plate for different initial angles of attack α_o are shown in Fig. 4 . From the sharp rise seen in the $\alpha_o = 0$ deg curve, the

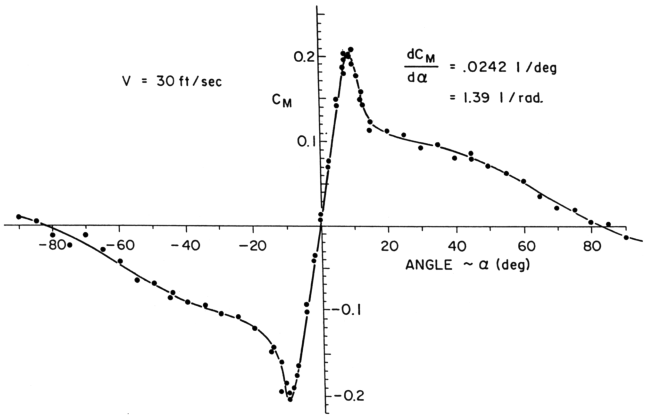

Fig. 2 Static aerodynamic moment characteristics.

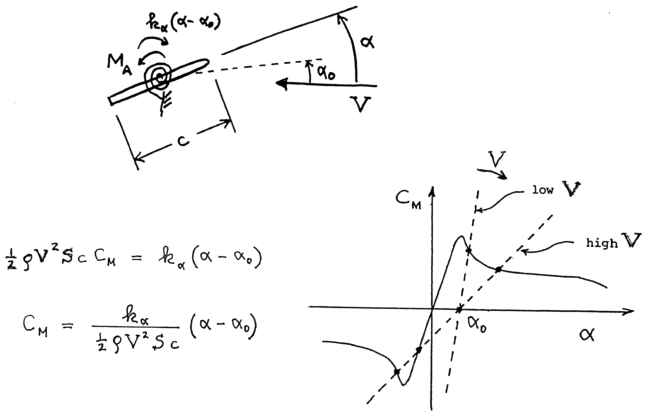

Fig. 3 Flat-plate divergence graphical solution.

linear static divergence speed V_D would occur around $V = 18$ ft/s, but stalling limits the infinite angles to finite values. Experimental values agree quite well with those calculated. It is noted that the graphical solution in Fig. 3 can give three solutions; however, the solution near $\alpha = 0$ deg is always statically unstable above the linear divergence speed V_D. Also, some of the static solutions above V_D were dynamically unstable and had to be lightly held in place to

[†]To standardize blockage effects at high angles of attack, the velocity for all of the subsequent static and dynamic tests was defined as that registered by the tunnel manometer when the plate section was brought to zero angle and the tunnel propeller power setting remained unchanged.

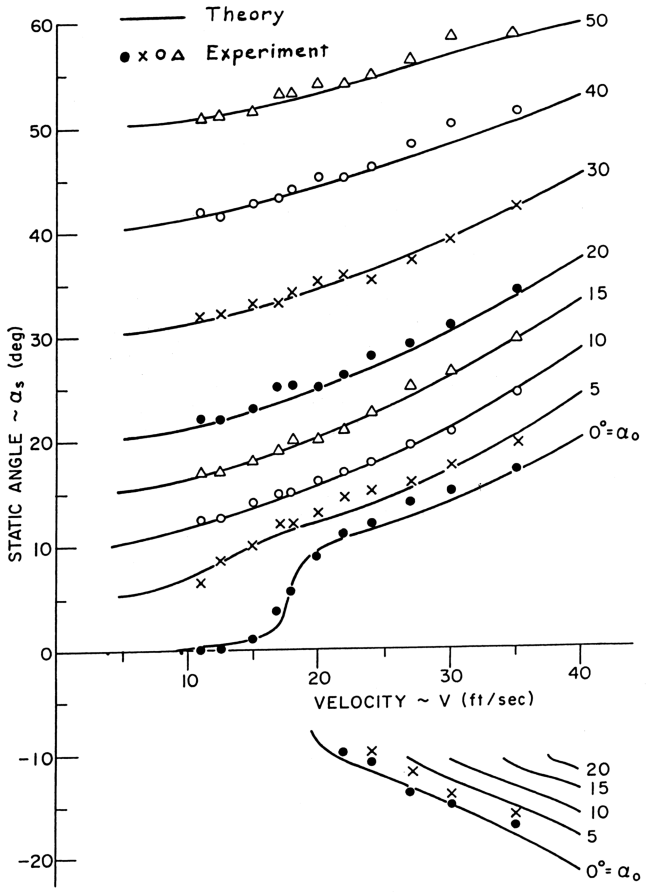

Fig. 4 Static divergence characteristics.

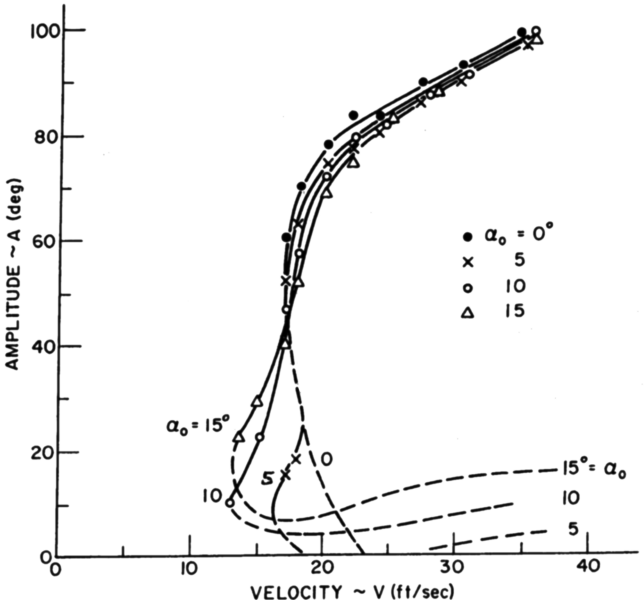

Fig. 5 Flutter amplitudes.

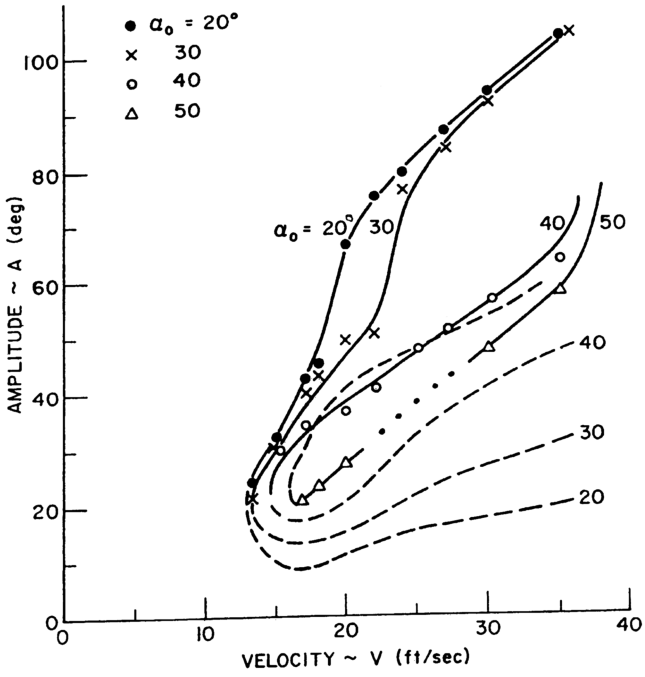

Fig. 6 Additional flutter amplitude.

prevent their dynamic oscillatory buildup. This will be discussed presently. Note also the general resemblance of Fig. 4 with the static postbuckling behavior of a simply supported flat plate with imperfections.

The torsional stall flutter behavior of the plate was investigated by setting the wing at an initial angle of attack α_o, then increasing the tunnel velocity in small increments. At each velocity, the wing was manually given various disturbance angles $\Delta\alpha$ from the static equilibrium position α_s, and the resulting transient position signal was recorded on an oscillograph. Also, the disturbance $\Delta\alpha$ needed to cause the wing to go into a steady flutter limit cycle was noted. Figure 5 shows the measured stall flutter amplitudes of the wing for initial angles of attack of $\alpha_o = 0$ to 15 deg. Stable limit cycles are shown by solid lines, and dashed lines indicate the $\Delta\alpha$ disturbance from the static equilibrium angle α_s needed to cause the oscillation. It is seen that amplitudes as large as 90 deg occurred. For initial angles $\alpha_o < 30$ deg, the oscillations took place roughly about the spring zero position α_o, rather than the static equilibrium position α_s. All of these large-amplitude limit cycles had a torsional frequency of about 8.0 Hz. For the $\alpha_o = 5$-deg case, two limit cycles of different amplitudes occurred near $V = 17$ ft/s, depending on the size of the initial disturbance $\Delta\alpha$. The smaller-amplitude limit cycle took place about the static equilibrium position α_s (i.e., going in and out of stall) at about 6.0 Hz, whereas the larger limit cycle oscillated about the spring zero position α_o at the usual 8.0-Hz value.

Figure 6 shows additional flutter amplitudes for initial angles of attack $\alpha_o = 20$ to 50 deg and also the disturbances $\Delta\alpha$ required to initiate the limit cycle from the static equilibrium position α_s. All of the static divergence positions α_s shown in Fig. 4 for these initial angles $\alpha_o = 20$ to 50 deg were dynamically stable here and would only go into a limit-cycle oscillation if given a large enough disturbance $\Delta\alpha$. The amount of disturbance seemed related to that needed to have the plate reach the stall peak.

Figure 7 shows a photograph of the large-amplitude limit cycle that occurred for the initial angle $\alpha_o = 0$ deg at $V = 17$ ft/s. Typical transient time histories taken for the $\alpha_o = 0$-deg case are shown in Fig. 8. At $V = 18$ ft/s, a small disturbance $\Delta\alpha = 35$ deg dies out, but a slightly larger disturbance $\Delta\alpha = 50$ deg causes a large-amplitude limit cycle. At $V = 30$ ft/s, the large-amplitude limit cycle develops as soon as the holding moment restraining the static equilibrium position $\alpha_s = 15$ deg is released.

For more information, a large moment of inertia I_o was added to the wing section outside the tunnel, which lowered the torsional frequency from 8.0 to 4.25 Hz, and the tests were repeated. Figure 9 shows the results of these tests. The large-amplitude limit cycles now occur at slightly lower speeds, and the small-amplitude limit cycles now also occur for $\alpha_o = 10$ and 15 deg as well as for $\alpha_o = 5$ deg. The increased inertia here seemed to allow for more ease in developing these small-amplitude limit cycles about the stall position.

An attempt was made to try to characterize the nonlinear limit-cycle behavior by examining the transient damping behavior of the

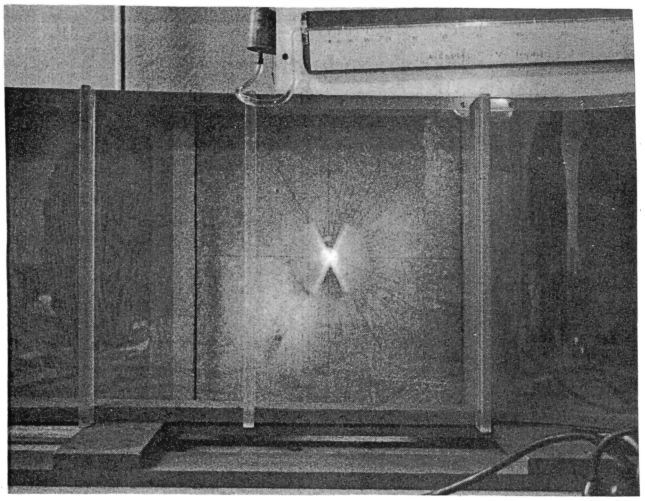

$\alpha_o = 0^\circ$ V = 17 FT/SEC

Fig. 7 Photo in the wind tunnel.

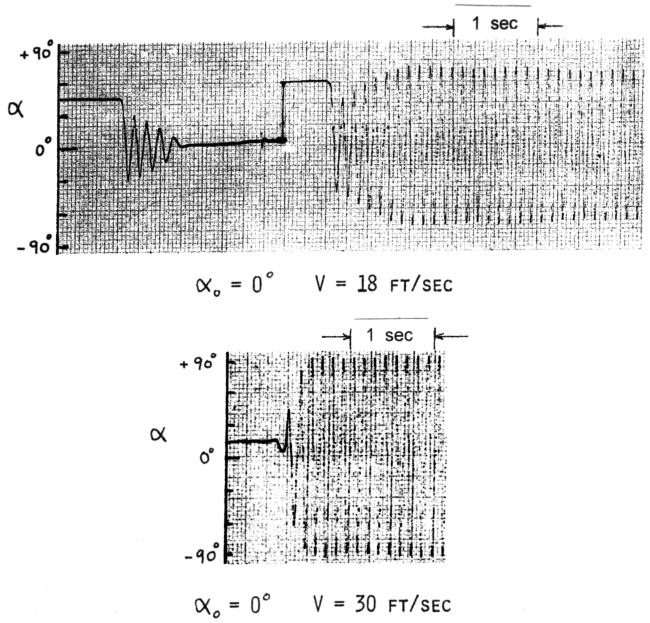

Fig. 8 Typical transient time histories.

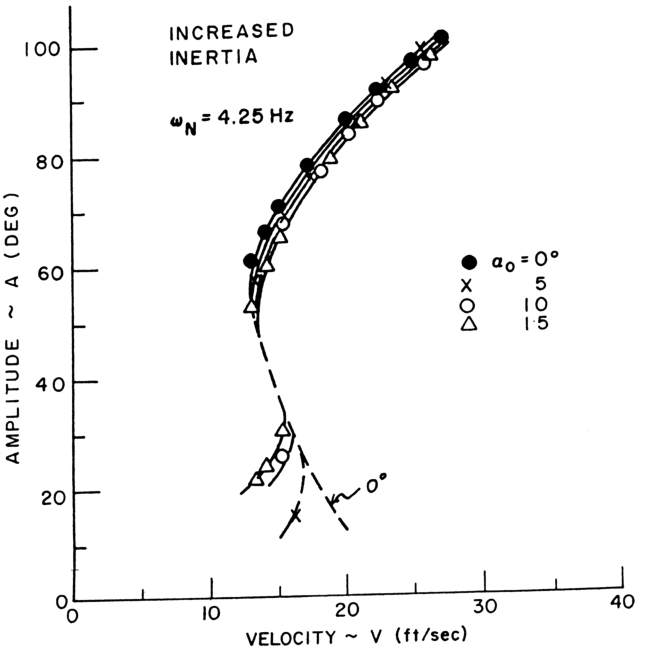

Fig. 9 Flutter amplitudes (increased inertia).

$$I\ddot{\alpha} + 2\zeta_F \omega_N I\dot{\alpha} + k_\alpha(\alpha - \alpha_o) = \tfrac{1}{2}\rho V^2 S c\left(m_o + m_1\alpha + m_2 \frac{b\dot{\alpha}}{V}\right)$$

$m_o, m_1, m_2 \rightarrow$ functions of $A, \alpha_o, \omega b/V$

or,

$$I\ddot{\alpha} + 2\zeta_T \omega I\dot{\alpha} + I\omega^2\alpha = I\omega^2\alpha_c$$

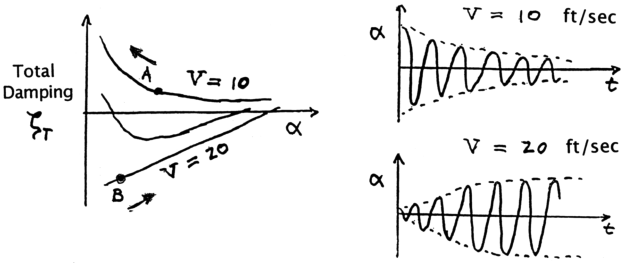

Fig. 10 Torsional vibrations and responses.

flat plate. Figure 10 gives the torsional vibration equation amended with a simple representation of the aerodynamic moment M_A, where the aerodynamic coefficients are nonlinear functions of amplitude A, initial angle α_o, and reduced frequency $\omega b/V$. Combining these terms with the standard torsional vibration terms gives the composite equation given next and also shown in Fig. 10:

$$I\ddot{\alpha} + 2\zeta_T \omega I\dot{\alpha} + I\omega^2\alpha = I\omega^2\alpha_c \tag{2}$$

where ζ_T represents the important total damping ratio. Estimates of this damping ratio ζ_T versus amplitude A obtained from transient-decay and increase records, such as in Fig. 8, are illustrated in Fig. 10. At $V = 10$ ft/s, the response dies out, at $V = 20$ ft/s, the response becomes a large-amplitude limit cycle, and at velocities in between, they illustrate the behavior shown in Fig. 8. Some results for ζ_T obtained from actual measured transient-decay records are shown in Fig. 11.

For interest, a simple test was made of the flat plate with the torsional spring removed. Figure 12 shows the resulting rotational speed of the plate f versus the velocity, which was very linear. This gave a Strouhal number $fc/V = 0.13$, which seems to correspond with that for vortex shedding of a stationary square section in an oncoming flow.

Finally, it should be mentioned that the torsional flutter assembly here was also tested later in a larger wind tunnel with upper and lower walls 36 in. apart instead of 15 in. to check possible wall effects. The same general behavior with large- and small-amplitude limit-cycle effects was again observed.

More extensive aerodynamic analysis of this simple torsional stall flutter problem by computational fluid dynamic (CFD) methods might reveal some of the fundamental characteristics and nonlinear behavior displayed here. For linear theory with no static or dynamic stalling present, the flat-plate wing pivoted at midchord is always dynamically stable. The basic investigation described here is from reports by Dugundji and Aravamudan [3] and Dugundji and Chopra [4]. A brief description is also found in additional references [5–7]. A video display of the flutter behavior shown here is included in a videotape by Strogatz [8]. A related display of smaller-amplitude

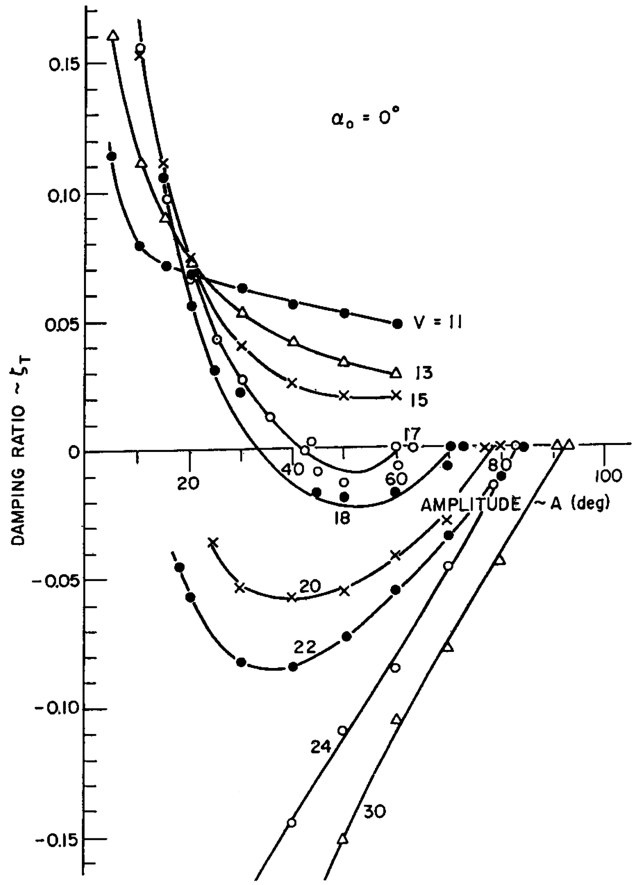

Fig. 11 Total damping estimates from transient-decay data.

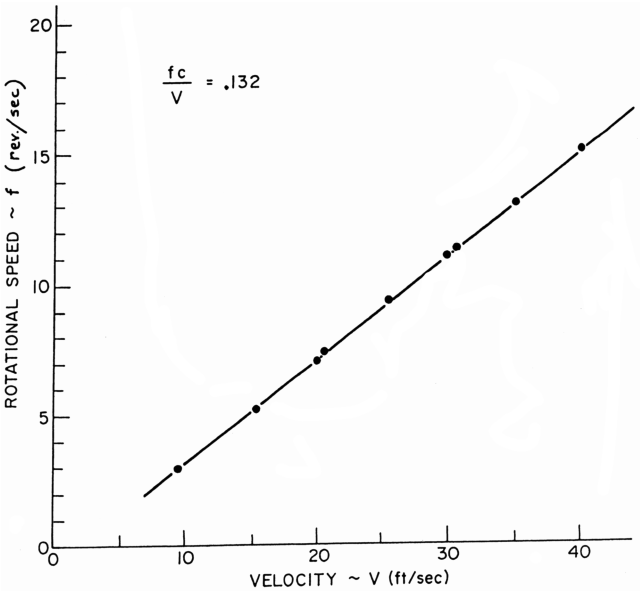

Fig. 12 Free rotation speeds of the flat plate.

nonlinear limit cycles with hysteresis is described by Tang and Dowell [9].

III. Nonlinear Vibrations of a Clamped Beam and a Buckled Beam

An investigation was made of an initially straight ($w_o = 0$) clamped–clamped beam with fixed immovable supports, subjected to a base harmonic excitation $w_B(t)$, as shown in Fig. 13. This is a

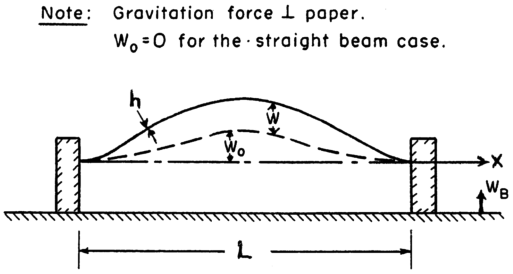

Fig. 13 Clamped beam subjected to base excitation w_B.

simple, easily achieved form of excitation and was investigated by Tseng and Dugundji [10–12], both experimentally and analytically. Because of the low damping in the beam, the experiment produced a jumble of vibrations everywhere. But later, slow and methodical observation, guided by analysis, gave a better understanding of the phenomena involved.

The governing differential equations are

$$EI\frac{\partial^4 w}{\partial x^4} - N_x\frac{\partial^2 w}{\partial x^2} = -m\left(\frac{\partial^2 w}{\partial t^2} + \frac{\partial^2 w_B}{\partial t^2}\right) - c\frac{\partial w}{\partial t}$$
$$N_x = N_o + \frac{EA}{2L}\int_0^L \left(\frac{\partial w}{\partial x}\right)^2 \mathrm{d}x \tag{3}$$

where N_o represents an initial tension in the beam and the integral term represents the additional nonlinear tension caused by the beam deflection. Applying harmonic base excitation, $w = w_{Bo}\sin\omega_F t$, and considering only the lowest fundamental bending vibration mode,

$$\frac{w}{h}(x,t) = \phi_1(x)q_1(t) \tag{4}$$

the application of Galerkin's method will result in

$$\frac{\mathrm{d}^2 q_1}{\mathrm{d}t^2} + 2\zeta\omega_1\frac{\mathrm{d}q_1}{\mathrm{d}t} + \omega_1^2 q_1 + K\omega_o^2 q_1^3 = 0.831\frac{w_{Bo}}{h}\omega_F^2\sin\omega_F t \tag{5}$$

where $\omega_o^2 = 501\ EI/mL^4$, $\omega_1^2 = \omega_o^2 + 12.31\ N_o/mL^2$, $K = 1.818$, and ζ is the critical damping ratio. Equation (5) is the well-known Duffing equation with its cubic nonlinear term and subjected to an acceleration-type forcing function. For calculation purposes, it is convenient to change to a new variable $q = q_1\omega_o/\omega_1$ and to introduce nondimensional time $n\tau = \omega_F t$, so that the basic equation reduces to

$$\frac{\mathrm{d}^2 q}{\mathrm{d}\tau^2} + 2\zeta n\sqrt{\alpha}\frac{\mathrm{d}q}{\mathrm{d}\tau} + n^2\alpha q + n^2\alpha K q^3 = 0.831 n^2 A_F\sin n\tau \tag{6}$$

where n is an integer, $\alpha = (\omega_1/\omega_F)^2 = 1/\Omega^2$, and $A_F = w_{Bo}\omega_o/h\omega_1$. General steady-state periodic solutions of this equation can be found in the form

$$q = y_o + \sum_{k=1}^{3}(x_k\sin k\tau + y_k\cos k\tau) \tag{7}$$

by applying the harmonic balance method and equating the constant, $\sin\tau$, $\cos\tau$, $\sin 2\tau$, $\cos 2\tau$, $\sin 3\tau$, and $\cos 3\tau$ terms separately to zero. This results in seven nonlinear equations in x_k and y_k. By suitable choice of n and k, this will yield simple harmonic, superharmonic (order 3, 2, and $\frac{3}{2}$), and subharmonic (order $\frac{2}{3}$, $\frac{1}{2}$, and $\frac{1}{3}$) solutions for the system. Simplified expressions for the harmonic, superharmonic, and subharmonic responses can be obtained by making assumptions on the magnitudes of x_k and y_k near appropriate frequencies, as indicated in [10–12]. More accurate solutions can be obtained by solving the nonlinear equations numerically by the Newton–Raphson method.

Figure 14 shows the analytic and experimental responses for a lightly damped, spring-steel beam. The beam was actually mounted and shaken horizontally to avoid static gravity effects. The beam had

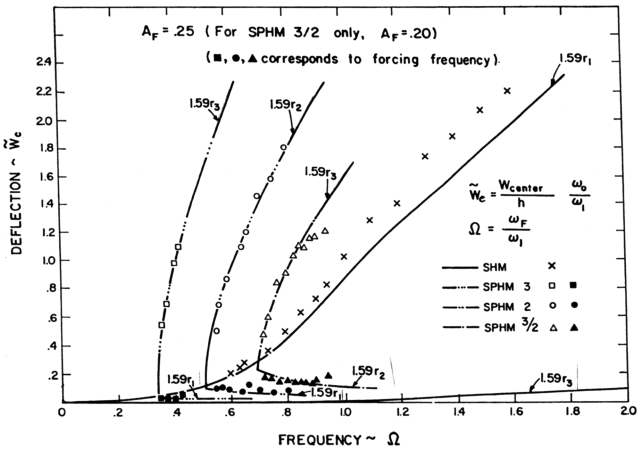

Fig. 14 Steady-state solutions (SPHM range).

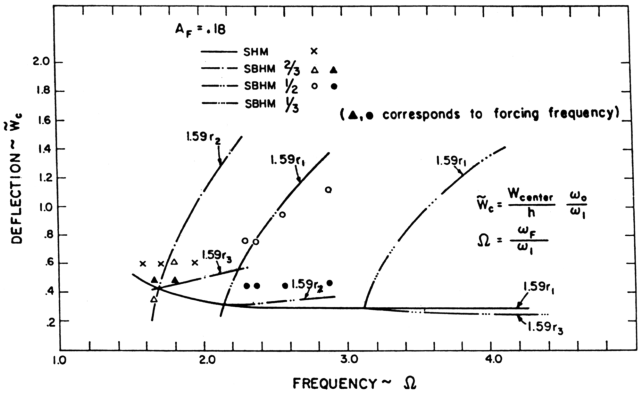

Fig. 15 Steady-state solutions (SBHM range).

a length of 18.0 in., a cross section of 0.021×0.5 in., a critical damping ratio of $\zeta = 0.0006$, and a basic first-mode frequency of $\omega_o = 13.4$ Hz, which was raised by initial tension to about $\omega_1 = 20$ Hz. In the figure, $r_i = \sqrt{x_i^2 + y_i^2}$ represents the nondimensional amplitudes q of the resulting periodic solutions, and $\tilde{w}_c = w_c\omega_o/h\omega_1 = \phi_1(L/2)q$ are the resulting amplitudes of oscillation. It is seen that in addition to the traditional hardening simple harmonic solution (SHM), a number of superharmonic solutions (SPHM) were also encountered analytically and experimentally for this lightly damped nonlinear system. These superharmonic solutions all tended to oscillate near the beam's natural frequency ω_1, rather than at the

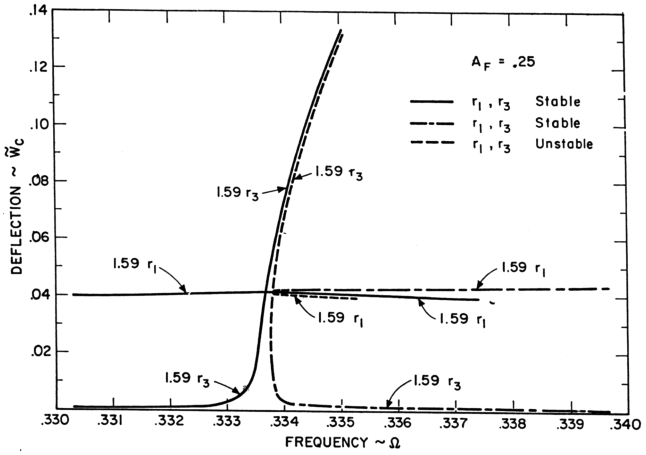

Fig. 16 Details of transition (SPHM order $m = 3$).

forcing frequency ω_F. The existence of possible multiple solutions for a given input frequency ω_F is an important feature of nonlinear systems, in contrast to the unique solution for a linear system. Subharmonic (SBHM) solutions were also encountered analytically and experimentally at higher forcing frequencies and are shown in Fig. 15.

For the small-amplitude forcing of these lightly damped systems, the superharmonic and subharmonic solutions can be approximated roughly by "shifted backbone curves." These can be obtained by using a single appropriate x_k solution from Eq. (7) and setting $A_F \approx 0$ and $\zeta \approx 0$ in Eq. (6). Solving Eq. (6) then yields roughly

$$q = x_k \approx \sqrt{\frac{4}{3K}[(m\Omega)^2 - 1]} \tag{8}$$

where $\Omega = \omega_F/\omega_1$, and $m = k/n$ is the order of the nonlinear oscillation. For example, the superharmonic of order $m = 3$ ($k = 3$ and $n = 1$) would develop for $\omega_F/\omega_1 > \frac{1}{3}$, as shown in Fig. 14. The actual details of the transition between the SHM and the SPHM solutions can be found by solving the seven nonlinear equations simultaneously by the Newton–Raphson method. This transition for the superharmonic order $m = 3$ case is shown in Fig. 16 and is seen to be continuous. In the solution, there also exists an unstable branch that is never physically realized. The same detailed behavior will also appear for all of the other SPHM and SBHM solutions here.

Figures 17 and 18 show some of the actual oscillograph records taken at various input frequencies and show clearly the experimental harmonic, superharmonic, and subharmonic responses of this lightly damped beam. The top trace is the beam response, and the lower trace gives the base motion. A summary of the main results here are shown

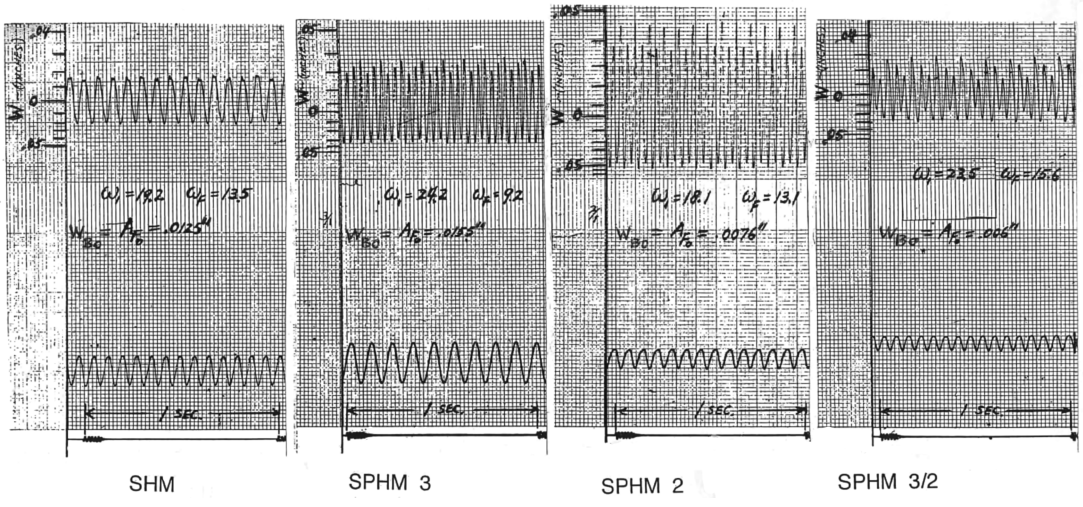

Fig. 17 SHM and SPHM responses.

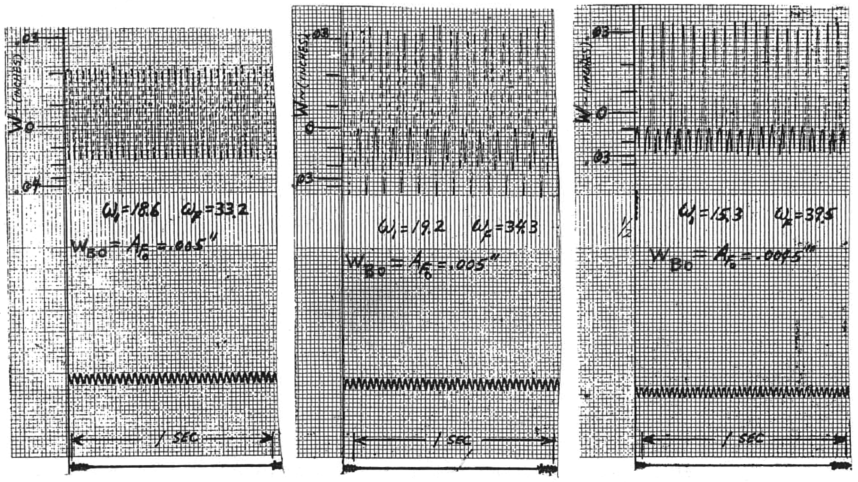

Fig. 18 SHM and SBHM responses.

in Figs. 14 and 15 and represented loosely by Eq. (8). Similar nonlinear vibration results were also found by Ehrich [13] in a study of the critical speeds of engine rotors and their subsequent vibrations. There, the nonlinearity arose from a bilinear stiffness of the rotor bearings in the vertical direction due to clearance effects.

Some rather interesting nonlinear effects are encountered if the ends of the clamped–clamped beam are brought together to buckle the beam into a shape w_o and it is then subjected to base excitation $w_B(t)$ (see Fig. 13). Such a buckling situation can occur by heating a beam clamped between two immovable supports. This problem was also investigated by Tseng and Dugundji [10,12]. The governing equations are now

$$EI\frac{\partial^4}{\partial x^4}(w+w_o)-N_x\frac{\partial^2}{\partial x^2}(w+w_o)=-m\left(\frac{\partial^2 w}{\partial t^2}+\frac{\partial^2 w_B}{\partial t^2}\right)-c\frac{\partial w}{\partial t}$$
$$N_x=-P_{\rm cr}+\frac{EA}{2L}\int_0^L\left[\frac{\partial}{\partial x}(w+w_o)\right]^2\mathrm{d}x-\frac{EA}{2L}\int_0^L\left(\frac{\partial w_o}{\partial x}\right)^2\mathrm{d}x \tag{9}$$

where $P_{\rm cr}=4\pi^2EI/L^2$ is the critical buckling load for this clamped–clamped beam. Applying harmonic base excitation as before and considering only the lowest bending mode, the additional deflection w is expressed as

$$\frac{w(x,t)}{w_o(L/2)}=\phi_B(x)\tilde{q}_1(t) \tag{10}$$

where now, $w_o(L/2)=ah=w_c$ is the initial center deflection, and the buckling mode shape $\phi_B(x)=(1-\cos 2\pi x/L)/2$ is used for both the initial shape and for the vibrations, instead of the previous $\phi_1(x)$. Note that $\phi_B(L/2)=1.0$ here. Applying Galerkin's method will result in

$$\frac{\mathrm{d}^2\tilde{q}_1}{\mathrm{d}t^2}+2\zeta\omega_1\frac{\mathrm{d}\tilde{q}_1}{\mathrm{d}t}+\omega_1^2\left(\tilde{q}_1+\frac{3}{2}\tilde{q}_1^2+\frac{1}{2}\tilde{q}_1^3\right)=\frac{4}{3}\omega_F^2A_F\sin\omega_F t \tag{11}$$

where $A_F=w_{Bo}/ah$ and $\omega_1^2=(8\pi^4EI/mL^4)a^2$. This gives vibrations w about the buckled beam centerline w_o. For vibrations relative to the original flat, unbuckled centerline, one can express the total deflection $w+w_o$ as

$$\frac{w+w_o}{w_o(L/2)}=\phi_B(x)[\tilde{q}_1(t)+1]=\phi_B(x)q(t) \tag{12}$$

Hence, $\tilde{q}_1+1=q$. Placing this relation into Eq. (11) and introducing nondimensional time $n\tau=\omega_F t$, the basic equation reduces to

$$\frac{\mathrm{d}^2q}{\mathrm{d}\tau^2}+2n\zeta\sqrt{\alpha}\frac{\mathrm{d}q}{\mathrm{d}\tau}-\frac{1}{2}n^2\alpha q+\frac{1}{2}n^2\alpha q^3=\frac{4}{3}n^2A_F\sin n\tau \tag{13}$$

for vibrations relative to the unbuckled flat position. This equation is seen to have two static equilibrium solutions, $q=+1$ and -1, corresponding to buckling on either side of the original flat, unbuckled centerline. Steady-state periodic solutions of Eq. (13) again take the form of Eq. (7), only now the constant term y_o must be included. However, the presence of the two-static equilibrium solutions may cause problems at certain levels of vibration.

A traditional steady-state harmonic SHM solution can be found for the beam with no damping by assuming from Eq. (7)

$$q=y_o+r_1\sin\tau \tag{14}$$

Placing this together with $n=1$ into Eq. (13) and applying harmonic balance will give

$$y_o^2=1-\tfrac{3}{2}r_1^2 \tag{15a}$$

$$\left[-\frac{\alpha}{2}-1+\frac{3\alpha}{2}y_o^2+\frac{3\alpha}{8}r_1^2\right]r_1=\frac{4}{3}A_F \tag{15b}$$

for the constant and $\sin\tau$ terms, respectively. Placing y_o^2 from Eq. (15a) into Eq. (15b) and recalling that $\alpha=1/\Omega^2$ and $\Omega=\omega_F/\omega_1$ results in the following cubic equation for amplitude r_1:

$$[1-\Omega^2-\tfrac{15}{8}r_1^2]r_1=\tfrac{4}{3}A_F\Omega^2 \tag{16}$$

Equation (16) is shown plotted in Fig. 19 for varying values of forcing function A_F. This is a traditional softening simple harmonic solution and is valid only for small amplitudes $r_1\le\sqrt{2/5}=0.632$, because this is where $r_1=y_o$, as seen from Eq. (15a), and the vibrations will not spill over into the other buckled region of the beam. At large amplitudes, one can assume that the beam is vibrating about both static equilibrium positions, so that one sets $y_o=0$ initially in Eq. (14). Placing this new q into Eq. (13) and applying harmonic balance for the $\sin\tau$ terms will now result in

$$[-\tfrac{1}{2}-\Omega^2+\tfrac{3}{8}r_1^2]r_1=\tfrac{4}{3}A_F\Omega^2 \tag{17}$$

These vibrations are also shown in Fig. 19 and represent a hardening simple harmonic solution, which is only possible for large amplitudes $r_1\ge\sqrt{4/3}=1.155$. At intermediate amplitudes, the beam would vibrate about either of the two static equilibrium positions and intermittently snap through from one to the other.

The analytic and experimental responses at small amplitudes of oscillation are shown in Fig. 20, when the beam is vibrating about one of the buckled static equilibrium positions. These buckled

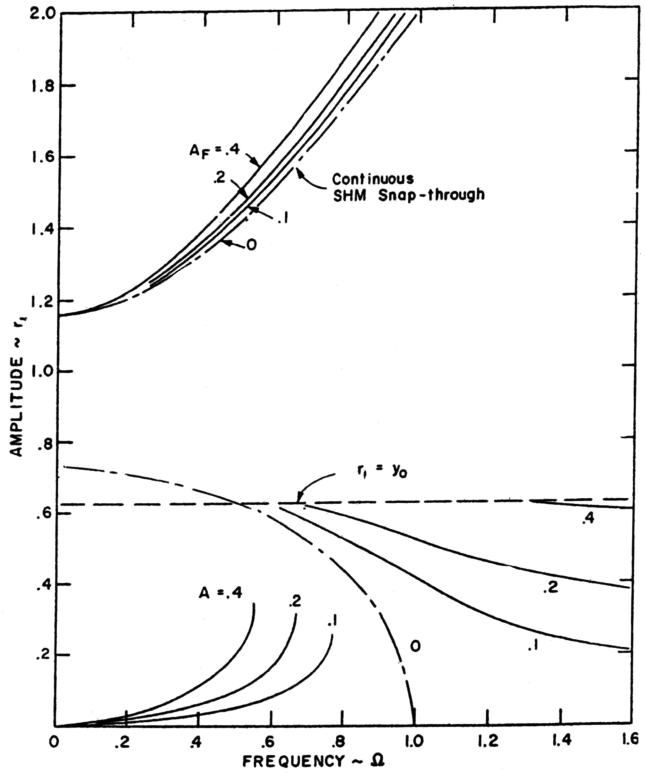

Fig. 19 Buckled beam: overall behavior of the SHM solution.

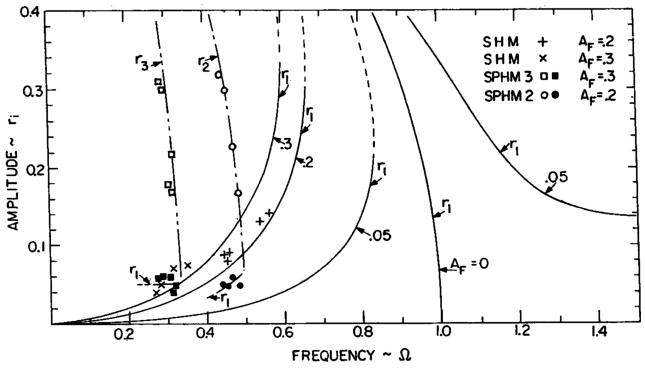

Fig. 20 Buckled beam: steady-state solutions.

positions were set at $a = 1.5$ (i.e., $w_o = 1.5h$), and the beam had an actual buckled frequency of 25.0 Hz. The beam is now a softening nonlinear system, and in addition to the traditional softening SHM, a number of SPHM were also encountered. The analytical and experimental responses here agreed well with one another. The superharmonic solutions encountered could again be estimated by shifted backbone curves by setting $A_F = 0$ and $\zeta = 0$ in Eq. (13) and using a single appropriate solution along with y_o from Eq. (7). Solving for y_o and r_k, as was done for the simple harmonic SHM solution in Eqs. (15a) and (15b), now results roughly in

$$q = r_k \approx \sqrt{\tfrac{8}{15}[1 - (m\Omega)^2]} \tag{18}$$

where $\Omega = \omega_F/\omega_1$, and the superharmonics now exist only for $\Omega < 1/m$. The continuous transition for the superharmonics of order $m = 3$ was again checked by a Newton–Raphson solution of the seven nonlinear equations as was done previously for the straight-beam case. Actual oscillograph records of the simple harmonic SHM and the SPHM 2 and SPHM 3 responses are shown in Fig. 21. These again clearly show the superharmonic character of this lightly damped beam ($\zeta = 0.0007$ here).

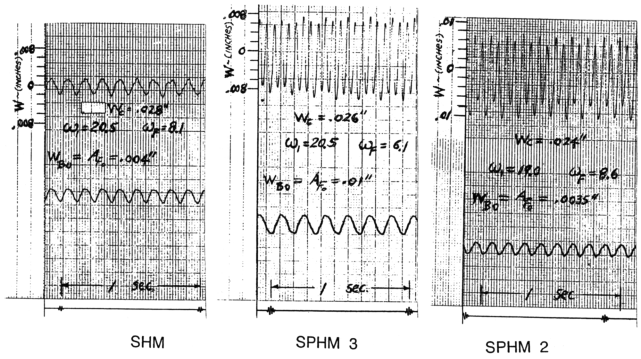

Fig. 21 Buckled beam: SHM and SPHM responses.

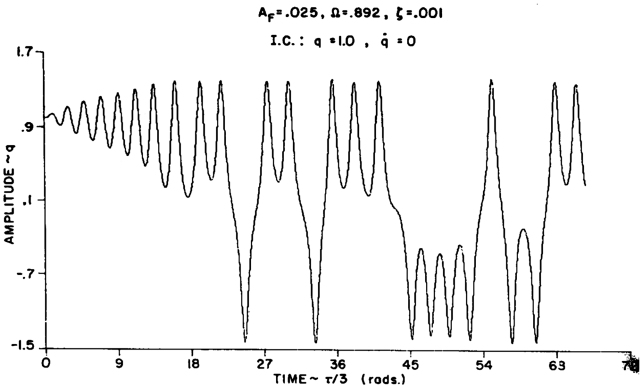

Fig. 22 Numerical SHM snap-through response

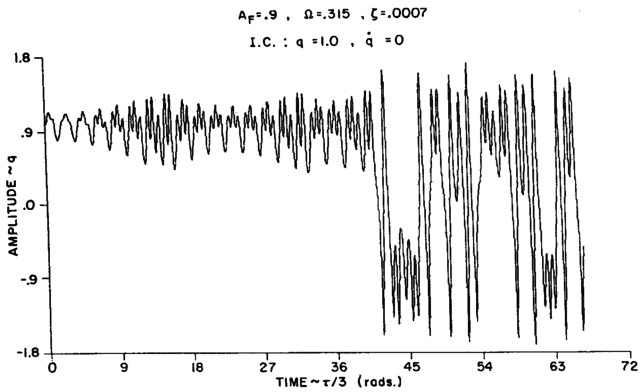

Fig. 23 Numerical SPHM 3 snap-through response.

To investigate the beam responses at intermediate amplitudes, Eq. (13) was integrated numerically by a Runge–Kutta method with a time increment of $\Delta\tau = 0.05$ for various forcing frequencies Ω and excitation amplitudes A_F. All integrations started from rest initial conditions, $q(0) = 1$ and $\dot{q}(0) = 0$. Figure 22 shows one such numerical response in which the beam attempts to develop SHM about one buckled position, but snaps through intermittently between the two static buckled positions. Figure 23 shows another such snap-through response, but here the beam develops SPHM 3 before snapping through intermittently. Experimental examples of this intermittent snapping through in both the harmonic and superharmonic cases are shown in Figs. 24 and 25.

The snap-through seems to occur as a dynamic overshoot of the attempt to reach the upper-branch solution near the jump points in the response (see Fig. 19). The approximate snap-through regions are presented in Fig. 26. The points here represent results of numerical integrations in which snap-through was first observed as the frequency Ω was increased for a given forcing amplitude A_F. The

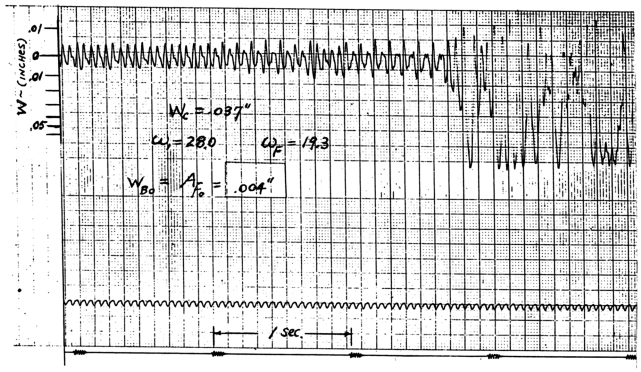

Fig. 24 Experimental SHM snap-through response.

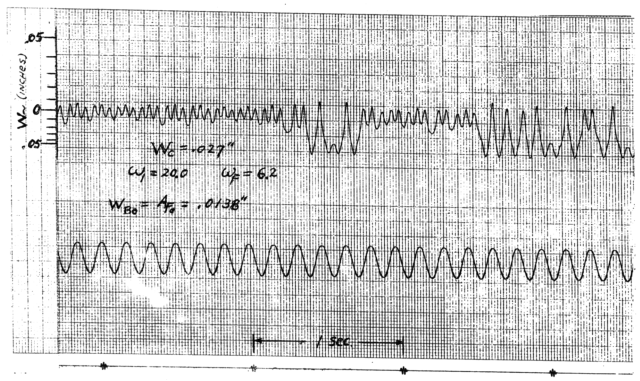

Fig. 25 Experimental SPHM 3 snap-through response.

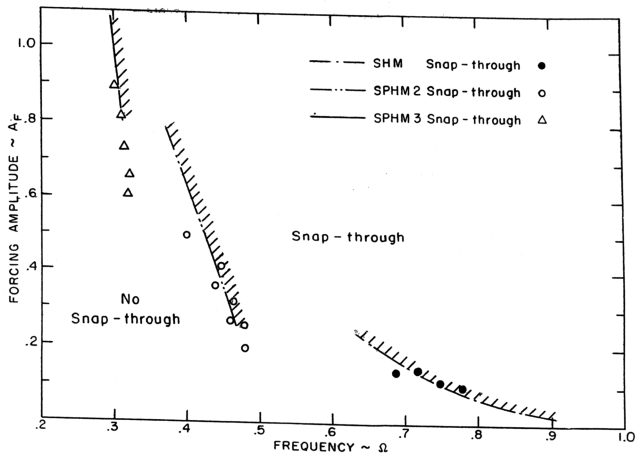

Fig. 26 Approximate snap-through regions.

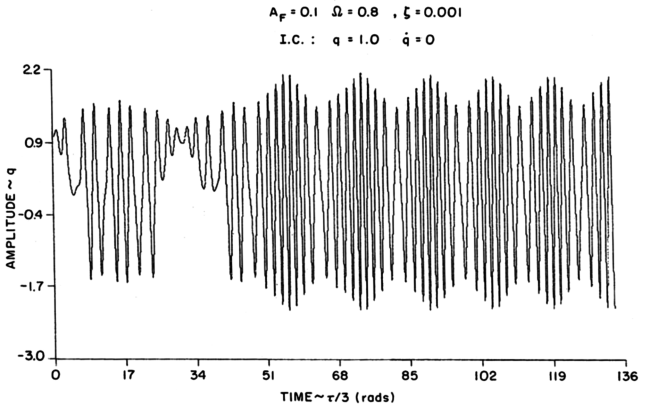

Fig. 27 Numerical continuous snap-through response.

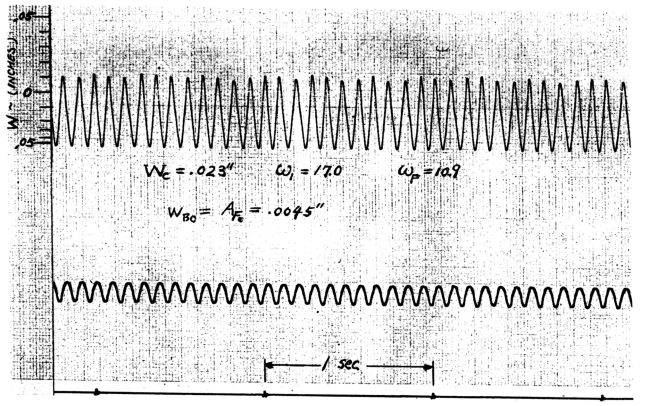

Fig. 28 Experimental continuous snap-through response.

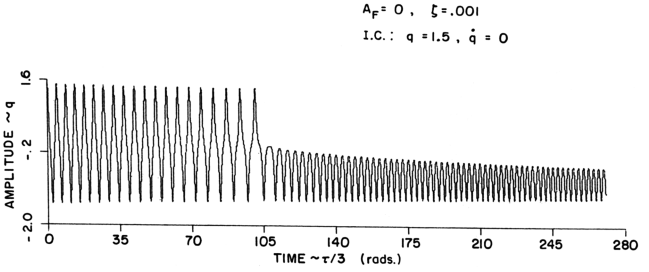

Fig. 29 Numerical free-vibration decay.

experimental results given in Figs. 20 and 21 all lie within the no-snap-through regions of this plot.

For large amplitudes, the beam can experience continuous harmonic snap-through about both static buckled positions, as described earlier by Eq. (17) and Fig. 19. This was also confirmed by numerical integration of Eq. (13), as shown in Fig. 27, and by actual experiment in Fig. 28.

For interest, the free-vibration decay of the large-amplitude oscillations from the continuous snap-through condition after the base motion is stopped was checked by numerical integration of Eq. (13) and is shown in Fig. 29. The decreasing frequency for the large amplitudes is followed by the increasing frequency of the small vibrations after snap-through to one side, as indicated by the $A_F = 0$ curve of Fig. 19. An experimental example of this free-vibration decay is shown in Fig. 30.

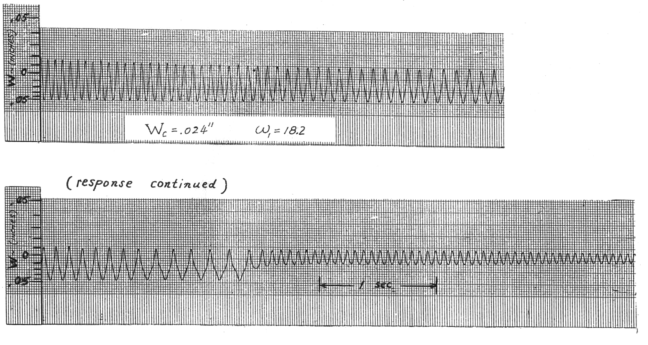

Fig. 30 Experimental free-vibration decay.

The experiment and analysis of this simple buckled beam constitute an early mechanical investigation into what is now termed "chaos" in nonlinear systems. There is much general literature on this subject (see, for example, Moon [14] and Nayfeh and Mook [15]). Further work and understanding of this specific problem is given by Dowell and Pezeshki [16], who investigated Eq. (13) analytically using chaos theory methods. Some of the analytical and experimental data regarding development of snap-through can be further explored. The general clamped-beam problem here also relates to the nonlinear flutter of panels in supersonic flow, which was first introduced by Dowell [17,18] and continued by Virgin and Dowell [19] and many others.

IV. Dynamic Stability of a Pendulum under Parametric Excitation

An investigation was made of a simple bar pendulum under vertical harmonic excitation of its pivot $w(t)$, as shown in Fig. 31. The pendulum has a single degree of freedom, a clear-cut nonlinearity, and it is excited parametrically [i.e., through time-varying the parameters (coefficients) of its differential equation rather than by adding an external right-hand-side forcing function to the equation]. This pendulum was investigated by Dugundji and Chhatpar [20–22] both experimentally and analytically and was stimulated by the extensive study by Bolotin [23] on this subject.

The governing differential equation here is

$$\frac{mL^3}{3}\frac{\mathrm{d}^2\theta}{\mathrm{d}t^2} + c\frac{\mathrm{d}\theta}{\mathrm{d}t} + \frac{mL^2}{2}\left(g + \frac{\mathrm{d}^2 w}{\mathrm{d}t^2}\right)\sin\theta = 0 \tag{19}$$

where the harmonic excitation occurs in the stiffness coefficient. Applying vertical harmonic excitation, $w = w_0 \cos\omega_F t$, and rearranging will result in

$$\frac{\mathrm{d}^2\theta}{\mathrm{d}t^2} + 2\zeta\omega_1\frac{\mathrm{d}\theta}{\mathrm{d}t} + \left[\omega_1^2 - \frac{3}{2}\omega_F^2\frac{w_o}{L}\cos\omega_F t\right]\sin\theta = 0 \tag{20}$$

where $\omega_1 = \sqrt{3g/2L}$ is the pendulum natural frequency, and ζ is the critical damping ratio. Upon introducing nondimensional time $2\tau = \omega_F t$ and retaining the first two terms in the series for $\sin\theta$, Eq. (20) is reduced to the basic form

$$\frac{\mathrm{d}^2\theta}{\mathrm{d}\tau^2} + 2\zeta\sqrt{a}\frac{\mathrm{d}\theta}{\mathrm{d}\tau} + [a - 2q\cos 2\tau]\left(\theta - \frac{1}{6}\theta^3\right) = 0 \tag{21}$$

where the nondimensional parameters $a = (2\omega_1/\omega_F)^2$ relate to the forcing frequency, and $q = 3w_o/L$ relates to the base vertical motion. Equation (21) is the nonlinear modified Mathieu equation, including effects of damping. It gives a reasonable approximation up to about $\theta = 1.2$ rad (70 deg). For the case of small oscillations, $\theta < 0.4$ rad (20 deg), the θ^3 term is neglected and it becomes the linear Mathieu equation. The initial conditions in Eq. (21) are often taken on displacement as at $\tau = \phi/2$, $\theta = \theta_o$, and $\mathrm{d}\theta/\mathrm{d}\tau = 0$, where $\phi = 0$ when θ_o is introduced at the top of the vertical base motion w, and $\phi = \pi$ when introduced at the bottom of the base motion w.

The linear Mathieu equation has been studied extensively in the past (see, for example, McLachlan [24] and Bolotin [23]). Generally, the linear version of Eq. (21) is transformed by the substitution

$$\theta(\tau) = e^{-\zeta\sqrt{a}\tau} f(\tau) \tag{22}$$

into the undamped standard Mathieu-equation form:

$$\frac{\mathrm{d}^2 f}{\mathrm{d}\tau^2} + [\bar{a} - 2q\cos 2\tau]f = 0 \tag{23}$$

where $\bar{a} = a(1 - \zeta^2)$. The general theory of this undamped Mathieu equation (23) indicates that certain combinations of q and $\bar{a}$ will lead to exponentially increasing oscillations (unstable solutions), whereas others lead to constant-amplitude oscillations (stable solutions). Figure 32 shows the well-known Strutt's diagram, which indicates the stable and unstable regions on a plot of $\bar{a}$ versus q. For low q,

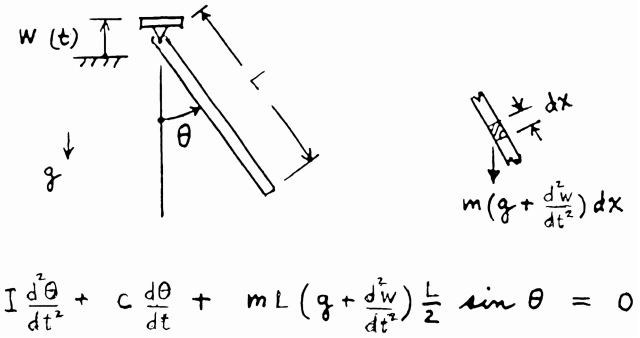

Fig. 31 Pendulum system.

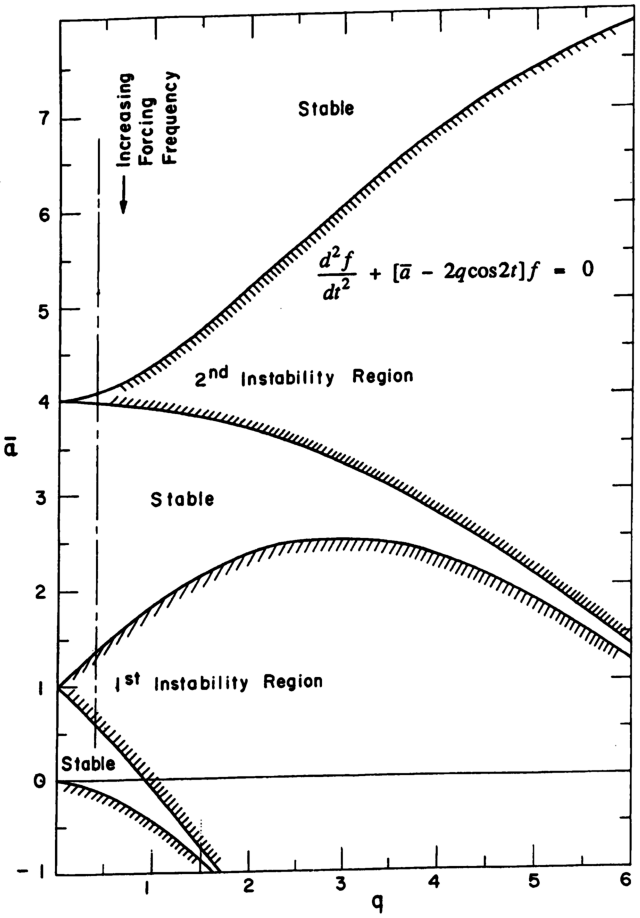

Fig. 32 Strutt's diagram for the Mathieu instability regions.

various instability regions develop near $\bar{a} = 1, 4, 9, 16$, etc. The first instability region near $\bar{a} = 1$ (i.e., $\omega_F = 2\omega_1$) is the widest and strongest. The presence of a small damping ζ will modify these undamped solutions by the transformation of Eq. (22) and thereby damp the stable regions and shrink the boundaries of the unstable regions. However, the first instability region remains the most significant and hence it will be the main one discussed here.

To investigate the behavior near the first instability region, the approach of Bolotin [23], using harmonic balance with his slowly varying amplitudes for this low-damped system, is applied to the complete nonlinear Eq. (21). Near this region, and for $q < 0.6$, one assumes

$$\theta = a_1(\tau)\sin\tau + b_1(\tau)\cos\tau \tag{24}$$

where $a_1(\tau)$ and $b_1(\tau)$ are slowly varying functions of time over the period 2π. Then

$$\dot{a}_1 2\pi/a_1 \ll 1, \qquad \ddot{a}_1 2\pi/\dot{a}_1 \ll 1 \tag{25}$$

where the dot notation $\dot{a}_1 = \mathrm{d}a_1/\mathrm{d}\tau$, etc., is used. Placing Eq. (24) into the basic Eq. (21), applying harmonic balance, introducing the conditions Eq. (25), and assuming the damping ratio $\zeta \ll 1$ will result in the two nonlinear first-order equations:

$$\dot{b}_1 - \frac{1}{2}(a-1+q)a_1 + \zeta\sqrt{a}b_1 + \left(\frac{a}{16}+\frac{q}{12}\right)a_1^3 + \frac{a}{16}a_1 b_1^2 = 0 \tag{26a}$$

$$\dot{a}_1 + \frac{1}{2}(a-1-q)b_1 + \zeta\sqrt{a}a_1 - \left(\frac{a}{16}-\frac{q}{12}\right)b_1^3 - \frac{a}{16}a_1^2 b_1 = 0 \tag{26b}$$

The total amplitude of the oscillation is then $A = \sqrt{a_1^2 + b_1^2}$.

Before dealing with these nonlinear equations, it should be mentioned that the solution of the linear Mathieu equation with damping can be obtained from Eqs. (26a) and (26b) by keeping only the linear terms in a_1 and b_1 in the equations. Then solutions of the form $a_1(\mathrm{t}) = a_1 e^{\sigma\tau}$ and $b_1(t) = b_1 e^{\sigma\tau}$ will result in a quadratic characteristic equation in σ, for which the roots are

$$\sigma = -\zeta\sqrt{a} \pm \tfrac{1}{2}\sqrt{-(a-1+q)(a-1-q)} \tag{27}$$

For the no-damping case $\zeta = 0$, the region between $a = 1-q$ and $a = 1+q$ will result in a positive real root σ and hence lead to unstable oscillations. For some damping present, the unstable region is diminished by the $-\zeta\sqrt{a}$ portion. In fact, if $\zeta\sqrt{a} > q/2$, the unstable oscillations disappear below this value of excitation q. Figure 33 shows the effect of damping on the first instability region. An approximation to these boundaries can result from setting $\sigma = 0$ in Eq. (27) and solving for a versus q for a given damping ζ. Also, it should be noted that outside the instability regions, one has $\sigma = -\zeta\sqrt{a} \pm i\nu$, and the decaying oscillations there have the two frequencies $1+\nu$ and $1-\nu$. This results in "beats" just outside the instability boundary and "waviness" farther away.

Turning now to the complete nonlinear Eqs. (26a) and (26b), one can obtain meaningful steady-state solutions where a_1 and b_1 are constants. For the no-damping case $\zeta = 0$, setting $\dot{a}_1$ and $\dot{b}_1$ equal to zero gives three such solutions by inspection; namely,

Trivial solution:

$$a_1 = 0, \qquad b_1 = 0 \tag{28a}$$

Solution 1:

$$a_1 = \pm\sqrt{\frac{a-1+q}{(a/8)+(q/6)}}, \qquad b_1 = 0 \tag{28b}$$

Solution 2:

$$b_1 = \pm\sqrt{\frac{a-1-q}{(a/8)-(q/6)}}, \qquad a_1 = 0 \tag{28c}$$

These solutions are shown plotted in Fig. 34 as the $\zeta = 0$ cases for a specific situation, where $q = 0.40$ and $\omega_1 = 1.37$ Hz. Subsequent investigation of the stability of these solutions showed that solution 1 is stable, solution 2 is unstable, and the trivial solution is unstable within the first linear instability region. Hence, only the stable solutions are physically realizable, and the infinite amplitudes of linear theory would end up as steady-state limit cycles on solution 1. The effects of small damping on these steady-state solutions can be found by again setting $\dot{a}_1$ and $\dot{b}_1$ equal to zero in Eqs. (26a) and (26b) and retaining the ζ terms. These nonlinear equations are now coupled and more difficult, but they can be solved numerically to give a_1 and b_1 for a given q, ζ, and a configuration using a Newton–Raphson or a

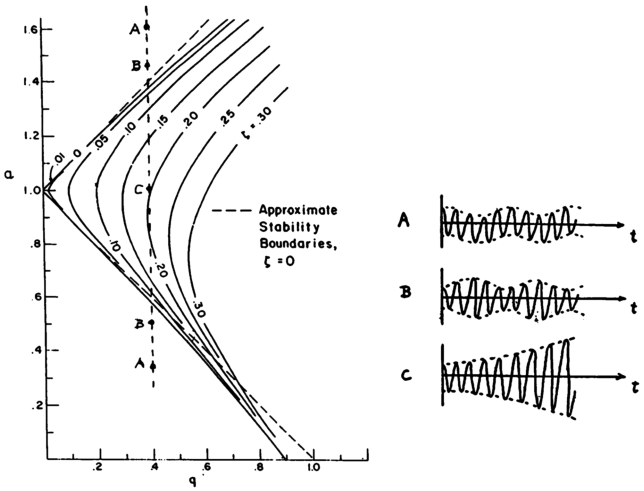

Fig. 33 Damping effects on the first instability region.

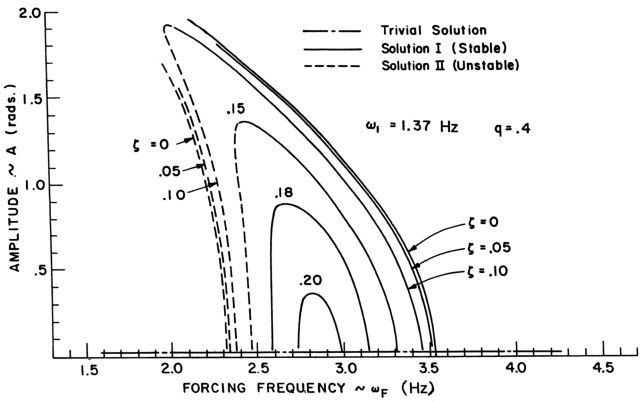

Fig. 34 Nonlinear steady-state solutions for the first instability region.

trial-and-error method. The results are shown in Fig. 34 for the specific q and ω_1 values previously mentioned. The stable and unstable portions of these solutions are indicated as well. These solutions disappear if sufficient damping is present. The transient behavior to get to these steady-state limit cycles can be obtained by numerically integrating the given Eqs. (26a) and (26b) subject to the displacement initial conditions mentioned previously. Together with Eq. (24), these initial conditions now become, at $\tau = \phi/2$, $a_1 = \theta_o \sin\phi/2$ and $b_1 = \theta_o \cos\phi/2$, where $\phi = 0$ for θ_o introduced at the top of the vertical base motion w, and $\phi = \pi$ when introduced at the bottom. In dealing with this transient behavior, it is noted that dividing Eqs. (26a) and (26b) gives

$$\frac{\mathrm{d}b_1}{\mathrm{d}a_1} = \frac{(a-1+q)a_1 - [(a/8)+(q/6)]a_1^3 - (a/8)a_1 b_1^2 - 2\zeta\sqrt{a}b_1}{-(a-1-q)b_1 + [(a/8)-(q/6)]b_1^3 + (a/8)a_1^2 b_1 - 2\zeta\sqrt{a}a_1} \tag{29}$$

The results of the numerical integrations can then be displayed to give much insight as a state-plane diagram that plots the trajectories in the a_1–b_1 plane at varying times τ. Such a technique was used by Weidenhammer [25] for similar types of equations. Figure 35 shows such a diagram for the case of $\omega_F = 2.20$ Hz, $q = 0.40$, and $\zeta = 0.01$. The radius to any point $\sqrt{a_1^2 + b_1^2}$ represents the amplitude $A(\tau)$ of the pendulum oscillations, and $\phi = 0$ and $\phi = \pi$ represent the top and bottom of the vertical motion w, respectively. A disturbance $\theta_o = 0.5$ rad introduced at the top ($\phi = 0$, $a_1 = 0$, and $b_1 = 0.5$) would decay to zero, whereas $\theta_o = 0.5$ introduced at the bottom ($\phi = \pi$, $a_1 = 0.5$, and $b_1 = 0$) would grow to the stable limit cycle at $a_1 = 1.90$. The three solutions for a_1 and b_1 given earlier by

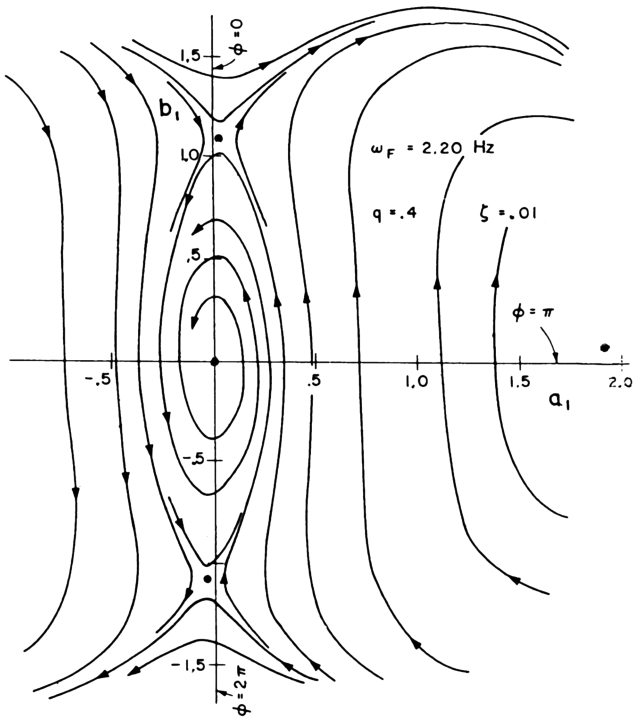

Fig. 35 State-plane diagram (first instability region), $\omega_F = 2.20$ Hz.

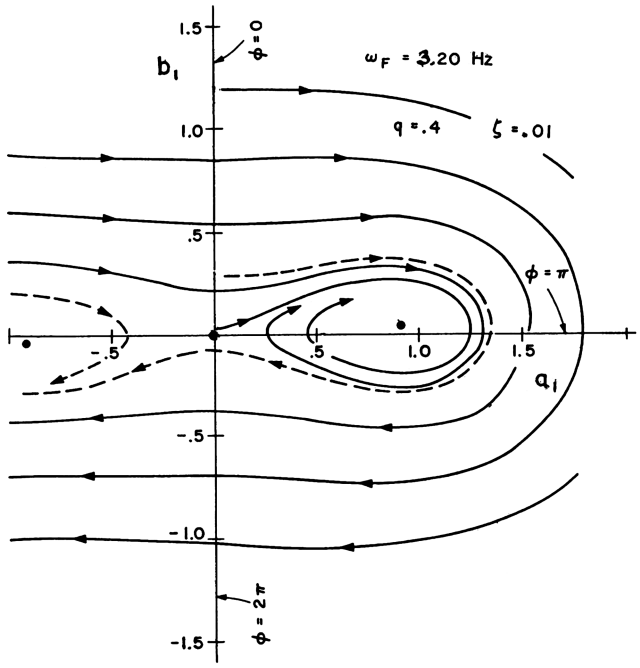

Fig. 36 State-plane diagram (first instability region), $\omega_F = 3.20$ Hz.

Eqs. (28a–28c) appear as singular points on this figure. Figure 36 shows the corresponding state-plane diagram for the case of $\omega_F = 3.20$ Hz, $q = 0.40$, and $\zeta = 0.01$. The saddle point at $b_1 = 1.10$ has now moved down to the origin, and all small disturbances θ_o grow to the stable limit cycle at $a_1 = 0.90$.

To investigate the behavior of the nonlinear modified Mathieu equation (21) near the second instability region of Strutt's diagram ($a = 4$; that is, $\omega_F = \omega_1$) and for $q < 1$, one assumes a solution

$$\theta = b_o(\tau) + a_2(\tau)\sin 2\tau + b_2(\tau)\cos 2\tau \tag{30}$$

and proceeds in the same manner as before (see [20]). For the purposes here, it is sufficient to note that the stable steady-state solution 1 for the second instability region at low values of q is given as

$$a_2 = \pm\sqrt{\frac{8}{a}(a-4)}, \qquad b_2 = b_o = 0 \tag{31}$$

similarly for the still-higher-instability regions. These instability regions are all much narrower, as seen in Fig. 32, and hence harder to excite for small q . Also, they are more easily eliminated by a small amount of damping ζ.

In addition to these previous limit cycles that develop near the first and higher instability regions of Strutt's diagram, other lesser-known subharmonic limit cycles may also develop in Eq. (21) for large-amplitude initial disturbances and small damping. These are generally found with fundamental frequencies equal to $\frac{1}{3}, \frac{1}{4}, \frac{1}{5}, \ldots$, of the forcing frequency ω_F. The $\frac{1}{4}$ subharmonic limit cycle will be discussed here.

For no damping present $\zeta = 0$, the $\frac{1}{4}$ subharmonic steady-state solution is assumed as

$$\theta = a_1 \sin\frac{\tau}{2} + a_3 \sin\frac{3\tau}{2} + a_5 \sin\frac{5\tau}{2} \tag{32}$$

where the constants a_3 and $a_5 \ll a_1$. Cubing the preceding θ and retaining only the first-order terms in a_3 and a_5 gives

$$\theta^3 \approx a_1^3 \sin^3\frac{\tau}{2} + 3a_1^2 a_3 \sin^2\frac{\tau}{2}\sin\frac{3\tau}{2} + 3a_1^2 a_5 \sin^2\frac{\tau}{2}\sin\frac{5\tau}{2} \tag{33}$$

Placing these into Eq. (21) and applying harmonic balance will result in three equations corresponding to the $\sin\tau/2$, $\sin 3\tau/2$, and $\sin 5\tau/2$ terms; namely,

$$\left[a - \frac{1}{4} - \left(\frac{a}{8} - \frac{q}{24}\right)a_1^2\right]a_1 + \left[q + \left(\frac{a}{8} - \frac{3}{8}q\right)a_1^2\right]a_3 + \left[-q + \frac{3}{8}qa_1^2\right]a_5 = 0 \tag{34a}$$

$$\left[q + \left(\frac{a}{24} - \frac{q}{8}\right)a_1^2\right]a_1 + \left[a - \frac{9}{4} - \left(\frac{a}{8} - \frac{q}{8}\right)a_1^2\right]a_3 + \left[\left(\frac{a}{8} - \frac{q}{8}\right)a_1^2\right]a_5 = 0 \tag{34b}$$

$$\left[-q + \frac{1}{8}qa_1^2\right]a_1 + \left[\left(\frac{a}{8} - \frac{q}{8}\right)a_1^2\right]a_3 + \left[a - \frac{25}{4} - \frac{a}{4}a_1^2\right]a_5 = 0 \tag{34c}$$

For nontrivial solutions of these equations, the determinant Δ must equal zero. Solutions were obtained numerically for a given base motion q by finding the value of $a = (2\omega_1/\omega_F)^2$ that made $\Delta = 0$ for specified values of a_1, starting from $a_1 = 0$. This provided the nonlinear backbone curve of the steady-state response. A typical result for the specific case here of $q = 0.40$ and $\omega_1 = 1.37$ Hz was $a = 0.20$ ($\omega_F = 6.13$ Hz), $a_1 = 1.00$, $a_3/a_1 = 0.17$, and $a_5/a_1 = -0.041$. The presence of a significant a_3 contribution is noted, which makes the response tend toward a square wave. For smaller values of q, the two-term contribution, and even a one-term contribution, could be taken for θ in Eq. (32).

If some damping ζ is present, both sine and cosine terms must be included for θ. For simplicity, the a_5 and b_5 terms are neglected here, and a steady-state solution is assumed as

$$\theta = a_1 \sin\frac{\tau}{2} + b_1 \cos\frac{\tau}{2} + a_3 \sin\frac{3\tau}{2} + b_3 \cos\frac{3\tau}{2} \tag{35}$$

where a_3 and $b_3 \ll a_1$ and b_1. Placing these again into Eq. (21), retaining only first-order terms when cubing θ, and applying harmonic balance will result in four nonlinear equations in a_1, b_1, a_3, and b_3 which can be solved by Newton–Raphson or trial-and-error methods [20]. Figure 37 shows these damped solutions for the specific case of $q = 0.40$ and $\omega_1 = 1.37$ Hz. These appear as U-

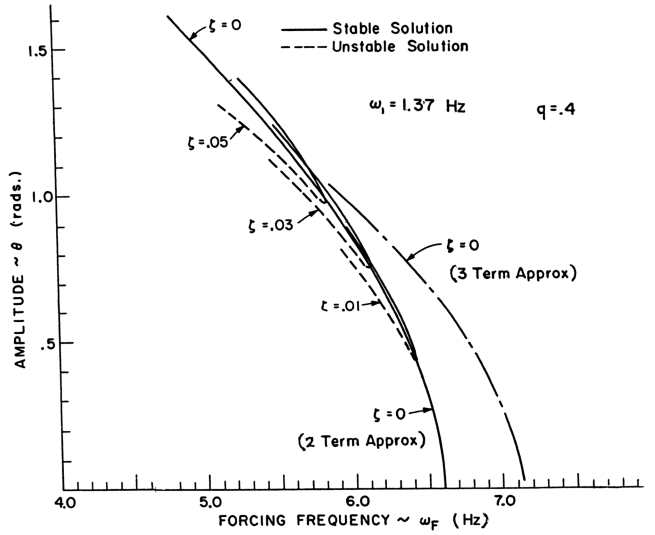

Fig. 37 Nonlinear steady-state solutions for the $\frac{1}{4}$ subharmonic.

shaped curves that disappear if sufficient damping is present. These are in contrast to the inverted U-shaped curves around the instability regions of the Mathieu equation (Fig. 34). The stable and unstable portions of these solutions are indicated, and the stable solution falls close to the no-damping backbone curve. A sufficient magnitude disturbance is required to achieve this $\frac{1}{4}$ subharmonic limit cycle when damping is present. These magnitudes can be explored more accurately if more terms are taken in the initial steady-state solution (35).

Other subharmonic limit cycles can be similarly achieved. For no damping present $\zeta = 0$, the $\frac{1}{3}$ subharmonic steady-state solution can be assumed as

$$\theta = a_1 \sin\frac{2\tau}{3} + a_2 \sin\frac{4\tau}{3} \tag{36}$$

whereas for the $\frac{1}{5}$ subharmonic, one can take

$$\theta = a_1 \sin\frac{2\tau}{5} + a_2 \sin\frac{4\tau}{5} + a_3 \sin\frac{6\tau}{5} + a_4 \sin\frac{8\tau}{5} \tag{37}$$

Similar development as for the $\frac{1}{4}$ subharmonic limit cycle will lead to corresponding results for these limit cycles (see [20]). For small values of the base motion parameter q, these subharmonic limit cycles can be expressed by fewer terms in their series approximation.

An experiment was performed on a simple bar pendulum to confirm these behaviors (actually, the experiment was done first and the theory was applied later to try to explain the observations). Figure 38 shows the experimental layout in which the pendulum was oscillated vertically by a Scotch yoke-type mechanism, run by a variable-speed motor through a belt and pulley. The angular deflection θ was measured by a potentiometer at the pivot and recorded by a two-channel recorder, which also recorded the frequency of oscillation. The pendulum itself was a steel rod, 8.0 in. long, and could swing through $\theta = \pm 96$ deg before hitting some stops. It was oscillated vertically with a base amplitude $w_o = 1.06$ in. ($q = 0.40$) for most of the runs. The pendulum linear natural frequency was measured as $\omega_1 = 1.37$ Hz, which agreed well with the linear relation $\omega_1 = \sqrt{3g/2L}$, whereas the critical damping ratio was measured from transient-decay rates at an average value of $\zeta = 0.01$ approximately. For large amplitudes, the pendulum frequency ω agreed well with the nonlinear theory relation:

$$\omega = \omega_1 \sqrt{1 - \tfrac{1}{8}\theta_o^2} \tag{38}$$

The experimental steady-state behaviors near the first instability region between $\omega_F = 2.3$ and 3.5 Hz is shown in Fig. 39. Inside this region, initial disturbances cause the response to either hit the stops

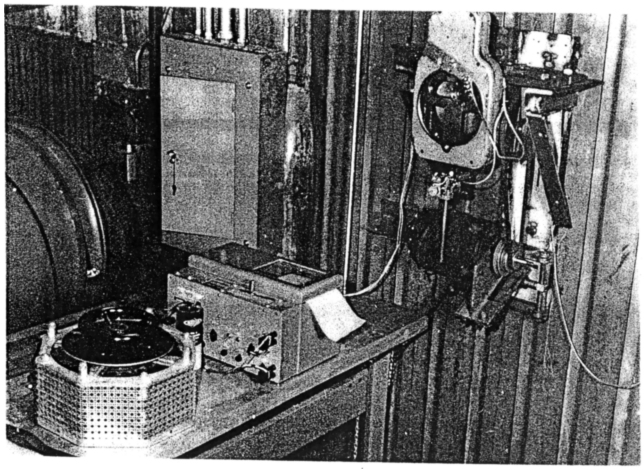

Fig. 38 Experimental pendulum layout.

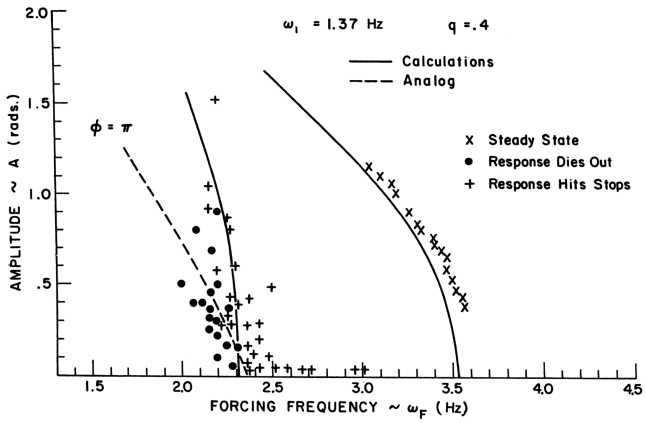

Fig. 39 Experimental steady-state near the first instability region.

or go to the stable limit cycle of Fig. 34. Outside the region, the response decays to zero. The unstable limit cycle acts as a rough divider between stable and unstable disturbances introduced at the top of the vertical base motion $w(\phi = 0)$, whereas the line for $\phi = \pi$ acts as the divider for disturbances introduced at the bottom of the base motion (see Fig. 35).

The experimental transient behavior near the first instability region is shown in Fig. 40. As the forcing frequency ω_F increases from 1.88 to 2.12 Hz, the change from waviness to beats is apparent. At $\omega_F = 2.67$ Hz, the response is well within the instability region and hits the stops at ± 96 deg, whereas at $\omega_F = 3.40$ Hz, the response settles into a steady limit cycle without hitting the stops. Outside the instability region at $\omega_F = 3.70$ and 4.40 Hz, the characteristic beats and waviness are again observed. This behavior agrees well with the analytical results characterized earlier by Eq. (27).

Some typical harmonic and subharmonic limit cycles are shown in Fig. 41. These show a harmonic response at $\omega_F = 1.29$ Hz (second instability region), a $\frac{1}{2}$ subharmonic at $\omega_F = 3.40$ Hz (first instability region), a $\frac{1}{3}$ subharmonic at 3.95 Hz, two $\frac{1}{4}$ subharmonics at 6.24 Hz and at 6.80 Hz, and a $\frac{1}{5}$ subharmonic at $\omega_F = 6.86$ Hz. To achieve these responses, large initial amplitudes had to be given, except for the $\frac{1}{2}$ subharmonic (first instability region), which is seen to start from very small disturbances. It is noted that the $\frac{1}{4}$ and $\frac{1}{5}$ subharmonic limit cycles can exist for approximately the same forcing frequency ω_F, depending on the initial disturbance given the system. All of these different limit cycles tend to have the pendulum oscillate near its natural frequency.

The overall steady-state response of the pendulum is summarized in Fig. 42, together with the experimental points. The experiments here confirmed the earlier theory and gave insight into the nonlinear

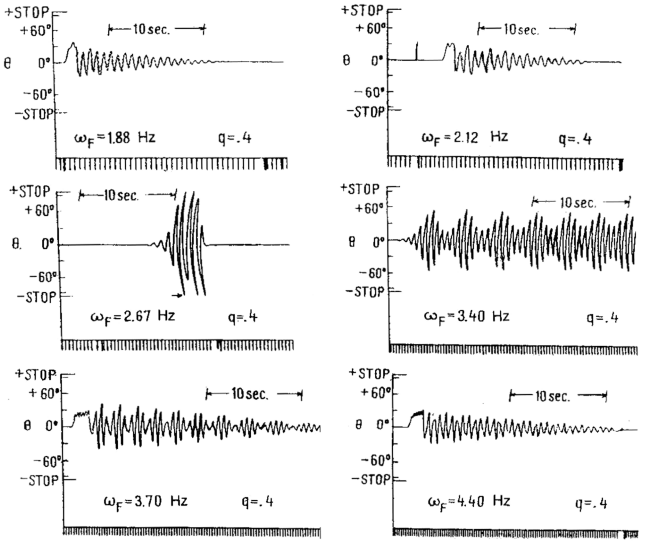

Fig. 40 Experimental transient response near the first instability region.

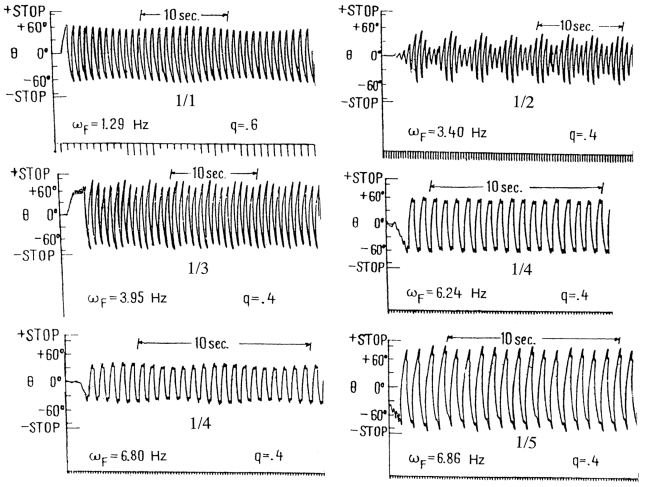

Fig. 41 Development of steady-state limit cycles.

behavior of the parametrically excited pendulum system. To achieve these responses, the system must have small damping and generally be given large initial disturbances. It is interesting to note that for very small values of the base motion parameter q, all of the limit cycles shown in Fig. 42 can be expressed by a simple one-term approximation in Eqs. (30), (32), (36), and (37), etc., which results in

$$\theta = \sqrt{8\left[1 - \left(m\frac{\omega_F}{\omega_1}\right)^2\right]} \tag{39}$$

where $m = \frac{1}{3}, \frac{1}{4}, \frac{1}{5}, \ldots$, for the subharmonic limit cycles, and $m = \frac{1}{2}, 1, 2, \ldots$, for the Mathieu-equation instability regions. This closely resembles the approximation found earlier for the superharmonic and subharmonic vibrations of the lightly damped, clamped beam [Eqs. (8) and (18)]. The $m = 1$ response of Eq. (39) is equivalent to the usual nonlinear backbone curve of Eq. (38), whereas the other cases for m represent shifted backbone curves themselves.

Further work by Chhatpar and Dugundji [21] explored the interaction of parametric and forced excitation using the same pendulum, with excitation $w(t)$ acting at an angle to the vertical direction. A good understanding of this single-degree-of-freedom pendulum is useful when dealing with the more difficult parametric and forced excitation of structures with their many degrees of freedom, their complex interactions, and their low dampings. See Bolotin [23] and, more recently, Nayfeh and Balachandran [26] and

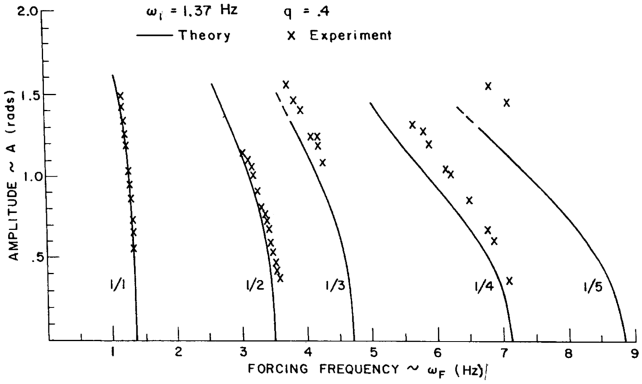

Fig. 42 Overall steady-state limit cycles.

Nayfeh [27], with their extensive studies of some of these further problems. Also see Dugundji and Mukhopadhyay [28] for a simple example of interacting bending-torsion beam vibrations under parametric excitation.

V. Conclusions

The flat-plate stall flutter, the clamped and buckled beam vibrations, and the parametrically excited pendulum all seemed simple problems that were easily modeled experimentally and analytically. They involved a single degree of freedom, and yet they revealed some fundamental and interesting characteristics of nonlinear aeroelastic and nonlinear vibrations of structures. In a way, these problems were all interrelated, with their common themes of limit cycles, multiple solutions, and disturbance-sensitive vibrations. The actual experiments corroborated and tended to focus the development of suitable analyses to explain the physical behavior. It is hoped that the investigations can provide useful basic understanding in more complex structural situations.

All of these investigations were done during the years 1968–1975 and were sponsored mainly by the U.S. Air Force Office of Scientific Research and in part by NASA. They were done with the analytical, numerical, and experimental tools of their time. With the vast increase in these tools during the past 35 years, better understanding of these nonlinear phenomena is possible now, as evident by current papers and investigations in the current literature. Some of the experimental data presented still remain to be resolved: for example, CFD analysis of the stall flutter behavior, more specific snap-through criteria for the buckled beam, damping and disturbance effects on the subharmonic limit cycles for the pendulum, excitation at an angle to the pendulum, etc.

Finally, I would like to end this paper by going back to C. P. Cavafy's poem, "Ithaca," mentioned at the beginning of this paper [1]. It commented on Odysseus' eventual return to Ithaca after his long ten-year journey from the Trojan War. The concluding lines go like this,

> Ithaca has given you the beautiful voyage.
> Without her you would never have taken the road.
> But she has nothing more to give you.
> And if you find her poor, Ithaca has not defrauded you.
> With the great wisdom you have gained, with so much experience,
> You must surely have understood by then what Ithacas mean.

References

[1] Cavafy, C. P., "Ithaca," *The Complete Collected Works of Constantine. P. Cavafy, translated by Rae Dalven*, Harcourt Brace, New York, 1961.

[2] Dugundji. J., "Personal Perspective of Aeroelasticity During the Years 1953–1993," *Journal of Aircraft*, Vol. 40, No. 5, Sept.–Oct. 2003, pp. 809–812.

[3] Dugundji, J., and Aravamudan, K., "Stall Flutter and Nonlinear Divergence of a Two-Dimensional Flat Plate Wing," Massachusetts Inst. of Technology, Aeroelastic and Structures Research Lab. TR 159-

6, Cambridge, MA, July 1974; also U.S. Air Force Office of Scientific Research 74-1734 TR, Arlington, VA, July 1974.

[4] Dugundji, J., and Chopra, I., "Further Studies of Stall Flutter and Nonlinear Divergence of Two-Dimensional Wings," Massachusetts Inst. of Technology, Aeroelastic and Structures Research Lab. TR 180-1, Cambridge, MA, June 1974; also NASA Langley Research Center CR-144924, Hampton, VA, –Aug. 1975.

[5] Dugundji, J., "Some Problems in Nonlinear Vibrations of Structures," Massachusetts Inst. of Technology, Space Systems Lab., Dept. of Aeronautics and Astronautics, Rept. SSL 2-88, Cambridge, MA, Jan. 1988.

[6] Dugundji, J., "Nonlinear Problems of Aeroelasticity," *Computational Nonlinear Mechanics in Aerospace Engineering*, edited by S. N. Atluri, Vol. 146, Progress in Aeronautics and Astronautics, AIAA, Reston, VA, 1992, pp. 127–155, Chap. 3.

[7] Dugundji, J., and Aravamudan, K., "Stall Flutter and Nonlinear Divergence of a Two-Dimensional Flat Plate Wing," *Revue Française de Mécanique Numero Special*, Societe Francaise de Mecaniciens, Paris, Oct. 1976, pp. 135–142.

[8] Strogatz, S., *Nonlinear Dynamics and Chaos: Lab Demonstrations* [video], Dept. of Theoretical and Applied Mechanics, Cornell Univ., Ithaca, NY, June 1995.

[9] Tang, D., and Dowell, E. H., "Limit-Cycle Hysteresis Response for a High- Aspect-Ratio Wing Model," *Journal of Aircraft*, Vol. 39, No. 5, Sept.–Oct. 2002, pp. 885–888.

[10] Tseng, W. Y., "Nonlinear Vibrations of Straight and Buckled Beams Under Harmonic Excitation," Massachusetts Inst. of Technology, Aeroelastic and Structures Research Lab. TR 159-1, Cambridge, MA, Nov. 1969; also U.S. Air Force Office of Scientific Research 69-2157 TR, Arlington, VA, Nov. 1969.

[11] Tseng, W. Y., and Dugundji, J., "Nonlinear Vibrations of a Beam Under Harmonic Excitation," *Journal of Applied Mechanics*, Vol. 37, No. 2, June 1970, pp. 292–297.

[12] Tseng, W. Y., and Dugundji, J., "Nonlinear Vibrations of a Buckled Beam Under Harmonic Excitation," *Journal of Applied Mechanics*, Vol. 38, No. 2, June 1971, pp. 467–476.

[13] Ehrich, F., "Nonlinear Phenomena in Dynamic Response of Rotors in Anisotropic Mounting Systems," *Journal of Mechanical Design*, Vol. 117(B), Special 50th Anniversary Design Issue, June 1995, pp. 154–161.

[14] Moon, F. C., *Chaotic Vibrations: An Introduction for Applied Scientists and Engineers*, Wiley, New York, 1979.

[15] Nayfeh, A. H., and Mook, D. T., *Nonlinear Oscillations*, Wiley, New York, 1979.

[16] Dowell, E. H., and Pezeshki, C., "On the Understanding of Chaos in Duffing's Equation Including a Comparison with Experiment," *Journal of Applied Mechanics*, Vol. 53, No. 1, Mar. 1986, pp. 5–9.

[17] Dowell, E. H., "Nonlinear Oscillations of a Fluttering Plate, Part 1," *AIAA Journal*, Vol. 4, July 1966, pp. 1267–1275.

[18] Dowell, E. H., "Nonlinear Oscillations of a Fluttering Plate, Part 2," *AIAA Journal*, Vol. 5, Oct. 1967, pp. 1856–1862.

[19] Virgin N. L., and Dowell, E. H., "Nonlinear Elasticity and Chaos," *Computational Nonlinear Mechanics in Aerospace Engineering*, edited by S. N. Atluri, Vol. 146, Progress in Aeronautics and Astronautics, AIAA, Reston, VA, 1992, pp. 531–546, Chap. 15.

[20] Dugundji, J., and Chhatpar, C. K., "Dynamic Stability of a Pendulum Under Parametric Excitation", Massachusetts Inst. of Technology, Aeroelastic and Structures Research Lab. TR 134-4; also U.S. Air Force Office of Scientific Research 69-0019 TR, Arlington, VA, Dec. 1968.

[21] Chhatpar, C. K., and Dugundji, J., "Dynamic Stability of a Pendulum Under Coexistence of Parametric and Forced Excitation," Massachusetts Inst. of Technology, Aeroelastic and Structures Research Lab. Rept. 134-5; also U.S. Air Force Office of Scientific Research 68-0001, Arlington, VA, Dec. 1967.

[22] Dugundji, J., and Chhatpar, C. K., "Dynamic Stability of a Pendulum Under Parametric Exciatation," *Revue Roumaine des Sciences Techniques. Série de Mećanique Appliquée*, Vol. 15, No. 4, July–Aug. 1970, pp. 741–763.

[23] Bolotin V. V., *The Dynamic Stability of Elastic Systems*, Gostekhizdat, Moscow, 1956, translated from Russian to English, Holden-Day, San Francisco, 1964.

[24] McLachlan, N. W., *Theory and Application of Mathieu Functions*, Dover, New York, 1964.

[25] Weidenhammer, F., "Das Stabilitatsverhalten der Nichtlinearen Biegeschwingungen des Axial Pulsierend Belasten Stabes," *Ingenieur-Archiv*, Vol. 24, 1956, pp. 53–68.

[26] Nayfeh, A. H., and Balachandran, B., *Applied Nonlinear Dynamics: Analytical, Computational, and Experimental Methods*, Wiley, New York, 1995.

[27] Nayfeh, A. H., *Nonlinear Interactions: Analytical, Computational, and Experimental Methods*, Wiley, New York, 2000.

[28] Dugundji, J., and Mukhopadhyay, V., "Lateral Bending-Torsion Vibrations of a Thin Beam Under Parametric Excitation," *Journal of Applied Mechanics*, Vol. 40, Sept. 1973, pp. 693–698.

B. Balachandran
Associate Editor